High-precision U-Pb zircon dating of late magmatism in the Samail ophiolite: A record of subduction initiation

Matthew Rioux[1,2,*], Joshua M. Garber[3], Michael Searle[4], Peter Kelemen[5], Sumio Miyashita[6], Yoshiko Adachi[7], Samuel Bowring[8]

[1] *Department of Earth Science, University of California, Santa Barbara, CA, 93106, USA*
[2] *Earth Research Institute, University of California, Santa Barbara, CA, 93106, USA*
[3] *Department of Geosciences, The Pennsylvania State University, University Park, PA 16803, USA*
[4] *Department of Earth Sciences, University of Oxford, Oxford, OX1 3AN, UK*
[5] *Department of Earth and Environmental Studies, Columbia University, Lamont Doherty Earth Observatory, Palisades, NY, 10964, USA*
[6] *Hokkaido Research Center of Geology, 58-7, Nopporo, Ebetsu, 069-0813, Japan*
[7] *Environmental Science Research Laboratory, Central Research Institute of Electric Power Industry, Abiko, Chiba, 270-1194, Japan*
[8] *Department of Earth, Atmospheric and Planetary Science, Massachusetts Institute of Technology, Cambridge, MA, 02139, USA*
[*] *corresponding author: rioux@eri.ucsb.edu*

Submitted manuscript

Published as:
Rioux, M., Garber, J. M., Searle, M., Kelemen, P., Miyashita, S., Adachi, Y., and Bowring, S. 2021, High-precision U-Pb zircon dating of late magmatism in the Samail ophiolite: A record of subduction initiation, *Journal of Geophysical Research*, v. 126, e2020JB020758, https://doi.org/10.1029/2020JB020758.

Key points

- High-precision U-Pb zircon dating constrains the timing of late magmatism within the Samail ophiolite
- The temporal and chemical evolution of the ophiolite is consistent with formation during subduction initiation
- The ophiolite chronology is similar to timescales of subduction initiation in geodynamic models and the Izu-Bonin-Mariana forearc

Abstract
Understanding the tectonic setting in which ophiolites form is necessary to determine how they can be used to study ocean spreading and subduction zone processes. Here we present high-precision U-Pb zircon dates and Sm-Nd isotopic data from two late magmatic series in the Samail ophiolite (Oman-United Arab Emirates), which constrain its tectonic development. Volcanic rocks in the ophiolite record a progression from MORB-like V1 lavas to subduction-related V2 lavas. Plutonic rocks related to V2 magmatism yielded $^{206}Pb/^{238}U$ dates of 95.557 ± 0.063 to 95.289 ± 0.067 Ma. A second late magmatic series consists of felsic dikes and sills that intermittently intrude the upper mantle and are attributed to melting of a subducting slab. These dikes in Oman range from 95.201 ± 0.032 to 94.95 ± 0.10 Ma, with $\varepsilon_{Nd}(t) = -5.05$ to -1.63. A single dike, attributed to V2 magmatism, has a higher $\varepsilon_{Nd}(t) = 7.35$ and a date of 95.478 ± 0.032 Ma. Similar intrusions in the UAE are younger, ranging from 94.119 ± 0.057 to 90.998 ± 0.052 Ma. Our new and existing data indicate the following timeline of ophiolite formation during subduction initiation: 1. Initial sole metamorphism at ≥96.2 Ma; 2. Formation of the crust through primarily decompression-related V1 magmatism from 96.1–95.6 Ma; 3. V2 magmatism related to H_2O-fluxed mantle melting from 95.6–95.2 Ma; and 4. Intrusion of slab-derived felsic dikes from 95.2–95.0 Ma. The temporal progression of magmatism is similar to the timescales of subduction initiation predicted by geodynamic models and observed in the Izu-Bonin-Mariana forearc.

1. Introduction

The Samail (Oman-UAE) ophiolite is the largest and best studied ophiolite in the world, and observations from the ophiolite have had a major impact on models for the structure and petrogenetic history of fast-spread oceanic lithosphere [e.g., *Boudier et al*., 1996; *Kelemen et al*., 1997; *Nicolas et al*., 1988; *Phipps Morgan and Chen*, 1993; *Quick and Denlinger*, 1993]. The tectonic setting during formation of the Samail and other ophiolites has long been controversial, with end-member models envisioning ophiolite formation at a normal mid-ocean ridge spreading center [*Boudier et al*., 1988; *Kusano et al*., 2017; *Nicolas and Boudier*, 2017] or in a supra-subduction zone setting [*Pearce et al*., 1981; *Searle and Malpas*, 1980; 1982]. Several lines of evidence now favor a supra-subduction zone origin for the Samail ophiolite, including the similarities between the major and trace element trends of the ophiolite lava series and subduction zone lavas [*Alabaster et al*., 1982; *Ishikawa et al*., 2002; *MacLeod et al*., 2013; *Pearce et al*., 1981; *Reagan et al*., 2017]; the identification of felsic dikes within the mantle section with continent-like isotopic signatures (negative ε_{Nd} and low ε_{Hf}), which have been attributed to melting of subducted sediments below the ophiolite [*Amri et al*., 2007; *Haase et al*., 2016; *Rioux et al*., 2013; *Rollinson*, 2009; *Rollinson*, 2015; *Spencer et al*., 2017]; thermobarometry from metamorphic rocks in the sole of the ophiolite that suggests peak metamorphism occurred at high pressures (1.0–1.3 GPa) in a subducting slab [*Cowan et al*., 2014; *Ghent and Stout*, 1981; *Gnos*, 1998; *Searle and Cox*, 2002; *Soret et al*., 2017]; and high-precision U-Pb zircon dating showing that metamorphism in some parts of the sole pre-dated, or was synchronous with, formation of the ophiolite crust [*Guilmette et al*., 2018; *Rioux et al*., 2016].

While these and other observations favor a subduction zone setting, the mechanisms of ophiolite formation and emplacement in such a setting remain incompletely understood. Proposed models envision ophiolite formation in both forearc [e.g., *Reagan et al*., 2017; *Stern and Bloomer*, 1992] and back-arc [*Pearce et al*., 1981] settings, and overlying mature subduction zones [*Searle and Cox*, 1999; 2002; *Searle et al*., 2015] or resulting from subduction initiation [*Agard et al*., 2020; *Reagan et al*., 2017; *Rollinson*, 2015; *Stern and Bloomer*, 1992]. Recently, the relative dates

of rocks from the metamorphic sole and ophiolite crust have been used to differentiate between competing models of subduction initiation [*Guilmette et al*., 2018; *Soret et al*., 2020], highlighting the importance of understanding the tectonic setting during ophiolite formation.

Here we present the results of a detailed study using high-precision U-Pb zircon dating and whole rock radiogenic isotopes to study the formation of the Samail ophiolite. To better constrain the tectonic development of the ophiolite, we focused on two late magmatic series that have been attributed to the development of subduction below the ophiolite: 1. Plutonic rocks related to the V2 magmatic event, and 2. Felsic dikes that intrude the ophiolite mantle just below the crust-mantle boundary. Our eighteen new high-precision dates (Figures 1, 2, and 3), combined with existing data (Figures 4 and 5), record the temporal progression from "MORB-like" magmatism during formation of the main volume of ophiolite crust, to the development of more pronounced "subduction-like" geochemical signatures in the later magmatic series. The data are consistent with models of ophiolite formation during subduction initiation, and provide direct temporal constraints on this critical but poorly understood process.

2. Geologic setting

The Samail ophiolite is exposed over approximately 20,000 km^2 in eastern Oman and the United Arab Emirates (Figure 1) [*Nicolas et al*., 2000]. The ophiolite preserves extensive exposures of a full oceanic crustal section and the uppermost mantle lithosphere. The mantle section (≤5 km thick) consists of residual harzburgite, with interspersed dunite pods and channels. The lower crust is predominantly olivine gabbro, with compositionally layered gabbros at the base (1–4 km) grading into foliated gabbros at higher structural levels (0.3–2 km). The foliated gabbros are overlain by a thin, discontinuous layer of evolved oxide gabbro, tonalite, trondhjemite, and quartz diorite (<1 km). These more evolved plutonic rocks intrude, and are intruded by, the sheeted dike complex, which is overlain by submarine basaltic pillows and flows (combined 1.5–2 km; thicknesses from Coogan et al. [2002] and Nicolas et al. [1996]). The entire ophiolite is thrust over a metamorphic sole, which preserves an inverted metamorphic gradient from amphibolite to granulite facies metabasalts and minor metasediment directly below the thrust to greenschist facies metasediments at lower structural levels. Estimated peak pressures and temperatures of sole metamorphism are 770–900ºC and 1.0–1.3 GPa for the rocks immediately beneath the ophiolite [*Cowan et al*., 2014; *Ghent and Stout*, 1981; *Gnos*, 1998; *Hacker and Mosenfelder*, 1996; *Soret et al*., 2017], corresponding to the HTa zone of Soret et al. [2017]. In the Bani Hamid area in the UAE, an out-of-sequence thrust sheet within the mantle section consists of amphibolite to granulite-facies marble, quartzite, calc-silicate, and minor amphibolite, with peak P-T conditions of 850 ± 60 ºC and 0.63 ± 0.05 GPa [*Searle et al*., 2015].

The volcanic rocks of the ophiolite can be divided into three series based on chemistry and stratigraphy. The V1 (Geotimes) pillows and flows occur directly above the sheeted dike complex. These lavas are the most chemically similar to mid-ocean ridge basalts [*Belgrano and Diamond*, 2019; *Belgrano et al*., 2019; *Ernewein et al*., 1988; *Godard et al*., 2006], although there are notable differences: V1 lavas have lower TiO_2 at a given MgO, higher average SiO_2, and depletions in Cr, Nb, and Ta relative to MORB [*MacLeod et al*., 2013; *Pearce et al*., 1981]. The V1 lavas are interpreted to represent the extrusive equivalent of the main portion of the intrusive crust [*Alabaster et al*., 1982; *Kelemen et al*., 1997; *Pallister and Knight*, 1981]. The overlying, younger V2 series are depleted in immobile incompatible trace elements (e.g., Nb, Ta, REE, Zr), and are chemically similar to some depleted subduction zone lavas [*Alabaster et al*., 1982; *Belgrano and Diamond*, 2019; *Belgrano et al*., 2019; *Ishikawa et al*., 2002; *Pearce et al*., 1981]. The upper

portion of the V2 series contains boninitic compositions [*Belgrano et al*., 2019; *Ishikawa et al*., 2002; *Kusano et al*., 2017]. The V2 series has been subdivided into the Lasail and Alley units. The Lasail unit consists of basaltic to andesitic rocks in focused centers in the northern part of the ophiolite [*Alabaster et al*., 1982], interpreted as remnant seamounts [*Alabaster et al*., 1982; *Pearce et al*., 1981]. The Alley unit is composed of primarily basaltic lavas and flows, which overlie both the V1 and Lasail extrusives [*Pearce et al*., 1981]. Several detailed studies have identified intrusive rocks related to V2 magmatism. The volume of V2 magmatism varies along the length of the ophiolite, with V2 volcanic and plutonic being rare in the southern ophiolite massifs and becoming increasingly more abundant to the north [*Goodenough et al*., 2010; *Haase et al*., 2016; *Styles et al*., 2006b]. Goodenough et al. [2010] argued that up to 50% of the crust in the UAE portion of the ophiolite is composed of V2 magmatism; however, detailed mapping and structural analyses by Ambrose and Searle [2019] suggest apparent differences between Oman and UAE may simply reflect the level of exposure. The final V3 volcanic series, which is enriched in LREE, is separated from the V2 lavas by a ~15 m thick pelagic sedimentary sequence and significantly post-dates ophiolite magmatism, potentially reflecting obduction of the ophiolite onto the continental margin [*Alabaster et al*., 1982; *Ernewein et al*., 1988].

A series of felsic dikes, sills, and plugs sporadically intrude the uppermost mantle and lowermost crust along the length of the ophiolite (mostly 1–10 m scale; Figure 1) [*Amri et al*., 2007; *Gass et al*., 1983; *Lippard et al*., 1986]. The occurrence of felsic dikes within mantle harzburgites is unexpected in the dominantly mafic ophiolite lithosphere and the dikes are geochemically distinct from the rest of the ophiolite. The field of major element data for the dikes overlaps the V1 and V2 volcanic and plutonic rocks, but stretches to significantly higher K_2O concentrations and the dikes are LREE enriched [*Rioux et al*., in review; *Rollinson*, 2009; *Rollinson*, 2014; 2015]. Further, the V1 and V2 magmatic series in the ophiolite have $\varepsilon_{Nd}(t) \approx +7–8$, similar to lavas at modern ridges [*Amri et al*., 2007; *Godard et al*., 2006; *Haase et al*., 2015; *McCulloch et al*., 1981; *Rioux et al*., 2012; *Rioux et al*., 2013; *Tsuchiya et al*., 2013]—with the exception of lower $\varepsilon_{Nd}(t)$ from upper V2 boninite lavas from the northern ophiolite massifs in Oman (+0.88 to +5.69) [*Kusano et al*., 2017]. In contrast, the felsic dikes have $\varepsilon_{Nd}(t) = -7.8$ to +7.8 (Figure 6) [*Amri et al*., 2007; *Briqueu et al*., 1991; *Cox et al*., 1999; *Haase et al*., 2015; *Lippard et al*., 1986; *Rioux et al*., 2013] and elevated $\delta^{18}O$ values [*Spencer et al*., 2017]. The negative $\varepsilon_{Nd}(t)$ values are consistent with input from continental rocks or terrigenous sediments. Based on these and other geochemical data, the intrusions are interpreted to have formed by three-component mixing between sediment and metabasalt melts generated near the top of a subducting plate, and a mantle component [*Haase et al*., 2015; *Pearce*, 1989; *Rioux et al*., 2013; *Rioux et al*., in review; *Rollinson*, 2009; *Rollinson*, 2014; 2015; *Spencer et al*., 2017]. There is significant overlap in the composition of the dikes from the Oman and the UAE sections of the ophiolite; however, the UAE dikes extend to more peraluminous compositions, including andalusite- and cordierite- (±garnet, biotite, tourmaline) bearing dikes [*Cox et al*., 1999; *Rollinson*, 2015].

In this study, we focused on plutonic rocks related to the V2 volcanic series and the low $\varepsilon_{Nd}(t)$ felsic intrusions that intrude the mantle and lowermost crust. We refer to plutonic rocks related to the different volcanic series as V1 or V2 plutonism—these rocks have been referred to as P1 and P2 in other studies [e.g., *Haase et al*., 2016]. For simplicity, we also refer to the isotopically evolved felsic dikes, sills, and plugs as simply felsic mantle dikes, although a small number of the dikes and sills intrude across the crust-mantle boundary into the lowermost crust.

3. Previous geochronology

Our research on the Samail ophiolite builds on previous U-Pb and K-Ar geochronology studies [e.g., *Goodenough et al*., 2010; *Hacker et al*., 1996; *Styles et al*., 2006b; *Tilton et al*., 1981; *Warren et al*., 2005]. These studies provided critical constraints on the timing of igneous crystallization and the cooling history of the ophiolite crust and underlying metamorphic sole. A summary of earlier studies can be found in Rioux et al. [2016].

Here, we summarize the results of high-precision U-Pb zircon dating from our previous work in the ophiolite, which provide an internally consistent dataset for comparison to our new results. All of the data from our published results [*Rioux et al*., 2012; *Rioux et al*., 2013; *Rioux et al*., 2016; *Searle et al*., 2015] and this study were collected using consistent analytical techniques in the Isotope Laboratory at the Massachusetts Institute of Technology (MIT), and the absence of inter-laboratory or decay constant biases (e.g., K-Ar versus U-Pb) make it possible to identify and interpret small, but significant, variations in dates. Sample locations and dates from all of our previous work are listed in Table 1 and sample locations are plotted in Figure 1.

We have previously published high-precision dates from 33 samples from the ophiolite crust and eight samples from underthrust metamorphic rocks (Figures 1, 4, 5) [*Rioux et al*., 2012; *Rioux et al*., 2013; *Rioux et al*., 2016; *Searle et al*., 2015]. There are resolvable ranges of dates in some of the studied samples, and here we report interpreted crystallization dates based on either i) the weighted mean $^{206}Pb/^{238}U$ date of the youngest cluster of overlapping dates within a sample, which defined an MSWD consistent with repeat measurements of a single population, or ii) the youngest single fraction $^{206}Pb/^{238}U$ date. The main V1 plutonic series in the Oman portion of the ophiolite exhibits weighted mean $^{206}Pb/^{238}U$ dates of 96.131 ± 0.050 to 95.64 ± 0.10 Ma (16 gabbros and 3 tonalite/trondhjemite; all reported $^{206}Pb/^{238}U$ dates are Th-corrected and have been recalculated to be consistent with the most recent tracer calibration and reduction parameters applied in this study) [*Rioux et al*., 2012; *Rioux et al*., 2013; *Rioux et al*., 2016]. Two additional V1 gabbros from the UAE portion of the ophiolite record overlapping dates of 95.742 ± 0.041 to 95.568 ± 0.043 Ma. Whole-rock Nd isotope data from nine V1 plutonic samples—eight dated and one undated—have $\varepsilon_{Nd}(t)$ = +7.43 to +8.28 [*Rioux et al*., 2012; *Rioux et al*., 2016], consistent with the range of values observed in V1 lavas and modern mid-ocean ridge basalts (Figures 6) [*Godard et al*., 2006; *Kusano et al*., 2012; *Kusano et al*., 2017; *McCulloch et al*., 1981].

We attribute ten previously studied samples to V2 magmatism. Four samples come from the Semail massif, including amphibole gabbro (9124M05) and tonalite/trondhjemite (9124M07, CWO18) intrusions just below the sheeted dike complex, and a tonalite plug (OM01-05) that intrudes the transition between layered and upper gabbro [*Rioux et al*., 2013]. Two additional samples come from a high-level amphibole gabbro (8130M01C) and tonalite (8130M02), in an area of abundant V2 magmatism in the Fizh massif. These six samples yielded weighted mean $^{206}Pb/^{238}U$ dates of 95.447 ± 0.092 to 95.240 ± 0.025 Ma. In this manuscript, we also re-categorize gabbro, gabbronorite, tonalite, and trondhjemite samples from the northern Rustaq (8121M04A, 8121M05) and southern Haylayn (8122M01, 8122M02) massifs as V2 plutonic rocks (Supplementary Text S1). Taken together, the eight V2 plutonic samples yield a total range 95.559 ± 0.075 to 95.240 ± 0.025 Ma—excluding lower precision data from 8121M04A and 8122M01 (Supplemental Text S1). Five of the studied V2 samples have whole rock $\varepsilon_{Nd}(t)$ = +7.19 to +8.83, which overlap with, but extend to lower values than, the analyzed V1 plutonic rocks [*Rioux et al*., 2013].

In our previous work, a single trondhjemite dike (9201M01) that intrudes harzburgite below the crust-mantle transition in the Haylayn massif yielded a weighted mean $^{206}Pb/^{238}U$ date of 95.191 ± 0.032 Ma and $\varepsilon_{Nd}(t)$ = –7.77; this is one of the series of felsic mantle dikes that are the

focus of the current study. One sample from our earlier work in the Samail massif— a tonalite dike (9127M01) that intrudes layered gabbro just above the crust-mantle transition—is probably also part of the same intrusive series. This lower crustal dike yielded $\varepsilon_{Nd}(t) = 6.90$ and a range of single grain dates; we interpret the youngest $^{206}Pb/^{238}U$ of 95.063 ± 0.062 Ma as the best estimate of the crystallization age. The relatively high ε_{Nd} of this sample, relative to other mantle dikes, likely reflects a large fraction of amphibolite-derived melt, as discussed in a companion paper in this volume [*Rioux et al.*, in review].

Finally, we have also previously studied amphibolite to granulite facies metamorphic rocks and associated cm-scale leucocratic pods from below the ophiolite. Leucocratic segregations from the well-studied Sumeini and Wadi Tayin metamorphic sole localities in Oman, which have previously been attributed to melting during metamorphism [*Cowan et al.*, 2014; *Searle and Malpas*, 1980; *Soret et al.*, 2017], yielded weighted mean $^{206}Pb/^{238}U$ dates of 96.169 ± 0.022 to 96.146 ± 0.035 Ma and 94.815 ± 0.030 to 94.69 ± 0.11 Ma, respectively [*Rioux et al.*, 2016]. A single garnet amphibolite (13222M08) from the Wadi Tayin sole locality yielded a range of dates from 96.067 ± 0.068 to 95.085 ± 0.063 Ma. Guilmette et al. [2018] reported single and multi-grain zircon data from a garnet amphibolite from the Wadi Tayin locality with a weighted mean $^{206}Pb/^{238}U$ date of 96.19 ± 0.14 Ma and a single multi-grain titanite analysis from the same rock with a date of 95.60 ± 0.27 Ma—the titanite date may be impacted by zircon inclusions, as argued by Garber et al. [2020]. Isotopic data from our previous work on the sole are variable: two garnet amphibolite samples from the Sumeini sole locality yielded $\varepsilon_{Nd}(t)$ = +3.90 to +7.11, while a leucocratic pod and metasediment from the Wadi Tayin sole locality gave $\varepsilon_{Nd}(t)$ = –7.01 and –8.35, respectively. Finally, a late, cm-scale vein that cuts the amphibolite foliation at Sumeini yielded a U-Pb date of 95.28 ± 0.24 Ma and $\varepsilon_{Nd}(t) = -11.04$, providing a minimum age for the formation of the metamorphic foliation. The older dates from the Sumeini sole locality are synchronous with or older than V1 magmatism in the ophiolite, consistent with metamorphism in a subducted plate during formation of the ophiolite crust in the overlying hanging wall. We note that ongoing work on the metamorphic sole suggests that U-Pb dates from leucocratic pods in the sole can be younger than U-Pb dates from nearby garnet amphibolites, and therefore provide minimum dates for the timing of prograde metamorphism (Rioux et al., unpublished). An amphibolite and plagioclase-amphibole dike from the Bani Hamid granulite block in the UAE yielded younger $^{206}Pb/^{238}U$ dates of 94.51 ± 0.12 and 92.574 ± 0.056 Ma, respectively (Table 2) [*Searle et al.*, 2015].

In summary, our existing zircon data suggest that V1 magmatism occurred from 96.1–95.6 Ma followed by V2 magmatism from 95.6 to 95.2 Ma. Two felsic mantle dikes from the Haylayn and Samail massifs yielded igneous crystallization dates of 95.2–95.1 Ma, with highly variable $\varepsilon_{Nd}(t) = -7.8$ to +6.9. Two metamorphic sole localities in Oman record dates of 96.2 and 94.8 Ma. The fact that the oldest metamorphic dates are synchronous with or pre-date the oldest V1 magmatism is consistent with metamorphism in a subducted slab during ophiolite formation in a supra-subduction zone setting.

The goal of this study was to determine the timing of V2 plutonism in areas that have been directly linked to V2 volcanism through detailed field and geochemical studies, and to date intrusion of felsic mantle dikes along the length of the ophiolite, to better understand the tectonic development of subduction below the ophiolite. Whole rock geochemical data from the dated felsic mantle dikes and a detailed discussion of the petrogenesis of the felsic dikes in Oman and the UAE is provided in a companion paper in this volume [*Rioux et al.*, in review].

4. Sample descriptions

4.1 *V2 plutonism—Oman*

To better constrain the timing of V2 magmatism in Oman, we analyzed samples from the Lasail, Fizh-South, and Wadi Rajmi intrusive complexes. As outlined above, we attribute several samples from our previous studies to V2 plutonism, based on field relations and the samples being younger than dated V1 plutonic rocks [*Rioux et al*., 2013]. In this study, we expanded on our earlier work by targeting areas where detailed mapping and geochemical analyses have identified different magmatic series, and directly linked the plutonic series to the V1 and V2 volcanic series [*Adachi and Miyashita*, 2003; *Tsuchiya et al*., 2013; *Usui and Yamazaki*, 2010]. The new samples are as follows: 1. In the Lasail plutonic complex, we dated a late quartz diorite intrusion (13216M05), which is interpreted based on its geochemistry to be related to the V2 Lasail volcanic unit (Figure 2a) [*Tsuchiya et al*., 2013]. 2. In the Fizh-South complex, a late, low-Ti magmatic suite intruded into the V1 plutonic crust. These rocks are chemically similar to, and interpreted to be the intrusive equivalent of, the V2 Alley volcanic series [*Adachi and Miyashita*, 2003]. We dated two samples from this suite: a m-scale tonalite dike that intrudes V1 dunite (08BU1) and a second m-scale tonalite dike that crosscuts V2 gabbronorites (12BU18; Figure 2d). 3. Finally, in Wadi Rajmi, V1 plutonic rocks were intruded by late km-scale ultramafic, gabbronorite, and tonalite bodies, and all units were subsequently cut by a boninitic dike swarm [*Usui and Yamazaki*, 2010]. We dated an oxide gabbronorite (04Raj150) from the later intrusive series (Figure 2c). We previously reported high-precision dates from V1 gabbros from both the Wadi Rajmi and Fizh-South complexes (Figures 1 and 4; 13215M07, 13215M09) [*Rioux et al*., 2016]. Locations for all of the samples in this study are provided in Table 2 and Figures 1 and 2.

4.2 V2 plutonism—United Arab Emirates

To constrain the timing of V2 plutonism in the UAE, we dated three tonalites and one gabbro from mapped exposures of the later intrusive series in the Aswad block. The late magmatic series in the UAE were mapped as the Bithnah and Fujairah gabbros [*Styles et al*., 2006b]. The two facies are distinguished based on outcrop-scale textures and field relations suggest they are coeval [*Styles et al*., 2006b]. These facies are interpreted to be equivalent to the V2 plutonic rocks in the Oman portion of the ophiolite. As discussed above, the late plutonic series comprises up to 50% of the exposed section in the UAE [*Goodenough et al*., 2010; *Styles et al*., 2006b]; however, this may reflect the level of exposure, rather than a higher proportion of V2 magmatism in this area [*Ambrose and Searle*, 2019]. The dated rocks include a sample of the Fujairah gabbro (131213M04), a sample from a km-scale tonalite intrusion associated with the Fujairah gabbro (131211M03), and two samples of tonalites from mixed mafic and felsic intrusions with 'vinaigrette' textures (131211M04, 131213M06; Figure 2b) [*Goodenough et al*., 2010; *Styles et al*., 2006b]. The 'vinaigrette' intrusions are associated with the Fujairah gabbro and consist of intimately intermingled tonalite and gabbro (Supplementary Figure S1). Sample 131213M06 comes from a vinaigrette exposure with lobate contacts between the mafic and felsic portions, suggesting coeval, immiscible liquids (Supplementary Figure S1a). The contacts are more angular for the vinaigrette exposure sampled by 131211M04, likely reflecting intrusion of a tonalite magma into a recently solidified gabbro (Supplementary Figure S1b, c). We previously reported a date from the V1 Kalba gabbro from the same area (Figure 2b and 5; 131213M02) [*Rioux et al*., 2016].

4.3 Felsic mantle dikes, Oman

We dated five felsic dikes that intrude the uppermost mantle and lower crust from the length of the ophiolite section in Oman. The dated samples are tonalites and trondhjemites, consisting of quartz + plagioclase ± biotite ± amphibole (Table 2). The sampled bodies intrude harzburgite or dunite just below the crust-mantle boundary (13211M02, 13215M08, 13217M01, 13221M05) or layered gabbros just above the boundary (13219M03; Figure 1).

4.4 Felsic mantle dikes, United Arab Emirates

We studied five felsic dikes that intrude the mantle section in the UAE. The dikes come from the Ra's Dadnah (MS13-5, 131204M02, 131204M03) and Wadi Hulw bin Sulayman (MS13-1, 131206M05) areas (Figure 1). The coastal Ra's Dadnah locality exposes a large composite sill, consisting of biotite-hornblende diorites to biotite granites, with a second peraluminous, leucocratic set of dikes containing tourmaline and spessartine garnet (± andalusite, cordierite, muscovite). Sample 131204M02 comes from a biotite tonalite, while MS13-5 comes from the second set of tourmaline-garnet leucogranites. Sample 131204M03 comes from a dike exposure inland, midway between Dadnah and Wadi Zikt, and is a biotite granite pegmatite. The Wadi Hulw bin Sulayman locality exposes a series of felsic dikes intruding into mantle harzburgite, adjacent to the Bani Hamid thrust sheet of granulite facies metamorphic rocks within mantle peridotite [*Searle et al.*, 2015]: sample 131206M05 is a biotite granite and MS13-1 is a garnet, muscovite, biotite leucogranite from this locality.

5. Methods and results

5.1 U-Pb zircon geochronology

High-precision single-grain U-Pb zircon geochronology was carried out by isotope dilution-thermal ionization mass spectrometry (ID-TIMS). All grains were dissolved using the chemical abrasion method [*Mattinson*, 2005], which preferentially removes damaged portions of the zircon prior to final digestion, minimizing or eliminating the impact of Pb loss on the final dates. Analytical procedures follow Rioux et al. [2012]. Dates reported and plotted throughout are corrected for initial exclusion of ^{230}Th from the ^{238}U decay chain. We assumed a melt Th/U equal to an average of modern mid-ocean ridge basalts for the V2 plutonic samples [*Rioux et al.*, 2015; *Rioux et al.*, 2016] and a $D_{Th/U} = 0.2$ with a 2-sigma uncertainty of ±40% for the felsic mantle dikes [*Hayman et al.*, 2019]. U-Pb data were reduced using the Tripoli and ET_Redux software packages [*Bowring et al.*, 2011; *McLean et al.*, 2011].

For simplicity, we will discuss the data in terms of interpreted crystallization ages, which are based on either a weighted mean date or—for more complex samples—the youngest precise date from the sample. Detailed discussions of the U-Pb systematics for each sample are provided in the Supplementary Text S1. The conclusions of this study do not change whether the crystallization age is estimated based on the weighted mean date or from the youngest fraction in each sample. Weighted mean plots for all of the dated samples are provided in Figure 3, interpreted crystallization ages are listed in Table 2, concordia plots are provided in Supplementary Figure S2, and U-Pb zircon data are in Supplementary Table S1.

We dated eight plutonic samples related to the V2 magmatic series in Oman and the UAE. Four samples from Oman yielded ^{206}Pb/^{238}U crystallization dates of 95.577 ± 0.063 to 95.336 ± 0.044 Ma. Three samples from the UAE yielded an overlapping range of ^{206}Pb/^{238}U dates from 95.50 ± 0.15 to 95.289 ± 0.067 Ma, while one additional sample (131213M04) yielded a slightly older date of 95.723 ± 0.081 Ma.

Five felsic dikes that intrude the upper mantle and lowermost crust in Oman (13211M02, 13215M08, 13217M01, 13219M03, 13221M05) yielded $^{206}Pb/^{238}U$ dates of 95.478 ± 0.032 to 94.95 ± 0.10 Ma. In contrast, five felsic dikes that intrude the mantle section in the UAE yielded significantly younger and more variable $^{206}Pb/^{238}U$ dates of 94.119 ± 0.057 to 90.998 ± 0.052 Ma.

Several of the dated samples have one or more analyses that predate the interpreted crystallization age of the sample. In six samples (13216M05, 13217M01, 13219M03, 13221M05, 131211M04, 131204M03), the anomalous zircon grains were 0.10 ± 0.07 to 0.63 ± 0.28 Ma older. In contrast, three samples (13211M02, 131213M04, MS13-1) each contained one anomalously old grain with a date of ~97 Ma, 1.4–3.2 Ma older than the crystallization ages of the samples.

5.2 Whole rock Sm-Nd isotopic geochemistry

Whole rock Sm-Nd isotopic data were collected at MIT following the procedures outlined in Rioux et al. [2012]. We analyzed 10 samples from Oman and the UAE (Figures 6; Supplementary Table S2). In Oman, the five dated felsic dikes that intrude into residual harzburgite and the lowermost layered gabbros yielded $\varepsilon_{Nd}(t)$ = –5.05 to +7.35. Two of the dated felsic mantle dikes from the UAE (MS13-1, MS13-5) yielded $\varepsilon_{Nd}(t)$ = –4.63 and –4.96, and one of the dated V2 tonalites (131211M03) from the crustal section in the UAE yielded $\varepsilon_{Nd}(t)$ = +7.39. Finally, an amphibolite and crosscutting diorite dike from the Bani Hamid metamorphic sheet in the UAE yielded $\varepsilon_{Nd}(t)$ = +2.09 and +0.91, respectively; high precision U-Pb zircon dates for the Bani Hamid samples were reported in Searle et al. [2015].

6. Discussion

6.1 Magmatic evolution of the Samail ophiolite

The new zircon U-Pb dates reported here, combined with our previous work, provide a detailed record of the magmatic evolution of the Samail ophiolite (Figure 4). In our previous studies, we demonstrated that plutonic rocks related to the V1 magmatic series in Oman crystallized from 96.1–95.6 Ma [*Rioux et al*., 2012; *Rioux et al*., 2013; *Rioux et al*., 2016]. This was followed by intrusion of inferred V2 related plutonic rocks from 95.6–95.2 Ma [*Rioux et al*., 2013]. The new dates presented in this paper from well-characterized exposures of V2 related plutonic rocks range from 95.6–95.3 Ma, consistent with our previous data. Our new and published data from the UAE portion of the ophiolite overlap the Oman dates: published dates from the V1 series in the UAE range from 95.7–95.6 Ma [*Rioux et al*., 2016] and three dates from V2 plutonic rocks reported here range from 95.5–95.3 Ma. A single V2 plutonic rock from the UAE has an older date of 95.7 Ma. This sample is from a mapped locality of late Fujairah gabbro; however, the date is older than three nearby V2 plutonic samples (Figure 2b)—a tonalite and two vinaigrette-textured intrusions—and we therefore suspect that the older sample may belong to the V1 intrusive series, and/or that it contains inherited zircon grains derived from V1 wallrocks. The absence of any systematic temporal variation from north to south in either the V1 or V2 plutonic rocks is consistent with the interpretation that the ophiolite formed along a fast-spreading, NNW-SSE oriented ridge system (present geographical reference frame) [*Rioux et al*., 2016].

The dated V2 plutonic rocks from Oman have been correlated with the Lasail and Alley units. Based on field relations and geochemistry, the Lasail unit has been interpreted to represent seamount activity or immature island arc volcanism predating eruption of the Alley unit [*Alabaster et al*., 1982; *Pearce et al*., 1981]. Our dates are inconsistent with this interpreted relationship: Sample 13216M05 is correlated with the Lasail volcanic unit [*Tsuchiya et al*., 2013] and yielded a date of 95.336 ± 0.044 Ma, while samples 08BU1 and 12BU18 are geochemically similar to the

Alley volcanic rocks [*Adachi and Miyashita*, 2003] and yielded older dates of 95.557 ± 0.063 and 95.540 ± 0.032 Ma, respectively. The inverted ages of the plutonic rocks may reflect a more protracted intrusive history for the Alley-type magmas prior to extensive eruptive activity; however, a larger dataset is needed to critically assess the relative timing of the intrusive magmatism related to the two series.

The felsic mantle dikes intruded toward the end of or slightly after the V2 magmatism. Four of the five dikes from Oman dated in this study yielded dates of 95.2–95.0 Ma and $\varepsilon_{Nd}(t) = -5.05$ to –1.63, consistent with the two Oman dikes we previously analyzed (95.2–95.1 Ma). We interpret the low $\varepsilon_{Nd}(t)$ and trace-element geochemistry of the dikes as evidence that they formed by sediment ± amphibolite melting on the top of a subducting plate [*Haase et al*., 2015; *Rioux et al*., 2013; *Rioux et al*., in review; *Rollinson*, 2009; *Rollinson*, 2014; 2015; *Spencer et al*., 2017]. A single dike (13217M01) yielded an older date of 95.5 Ma and a higher $\varepsilon_{Nd}(t) = +7.35$ (plotted as a yellow triangle in Figure 6). The date, $\varepsilon_{Nd}(t)$, and trace element geochemistry are all similar to V2 plutonic rocks within the ophiolite; the dike is LREE depleted and shows Nb, Ta, and Th depletions and Pb and Sr peaks on mid-ocean ridge basalt normalized extended trace element diagrams. Notably, the dike lacks the U- to V-shaped or LREE enriched REE patterns observed in most of the other dikes, which we attribute to amphibolite and/or amphibolite + sediment melting on the subducted slab. We instead attribute this dike to crystallization of a V2 magma within the upper mantle. Geochemical data for this sample and a more detailed discussion of its petrogenesis—and the petrogenesis of the other high $\varepsilon_{Nd}(t)$ dikes (Figure 6)—are provided in Rioux et al. [in review].

There is significant offset in dates between the felsic mantle dikes from Oman and the UAE. The five dikes from the UAE yielded dates of 94.1–91.0 Ma, postdating all of the crustal magmatism in the ophiolite and the Oman felsic mantle dikes. The two samples from Wadi Hulw bin Sulayman yielded dates of 94.119 ± 0.057 and 93.613 ± 0.044 Ma. These dates overlap the range of ages from the adjacent Bani Hamid metamorphic sheet (94.5–92.6 Ma) [*Searle et al*., 2015] and the dikes are likely related to melting during peak metamorphism of Bani Hamid. The two samples from the large composite dike at Ra's Dadnah yielded dates of 92.361 ± 0.026 Ma (marginal leucogranite; MS13-5) and 91.292 ± 0.061 Ma (biotite tonalite; 131204M02), suggesting the dike swarm was assembled by multiple intrusive episodes. The final sample from west of Ra's Dadnah yielded a date of 90.998 ± 0.052 Ma. The date is similar to the Ra's Dadnah tonalite and this locality likely represents a coeval, along strike intrusion.

As previously noted, several samples from geographically diverse locations had one or more anomalously old zircon grains, which are tens of thousands to millions of years older than the youngest population in the sample. Three samples have the oldest inherited grains with dates of ~97 Ma; a V2 gabbro from the UAE, a trondhjemite mantle dike from Oman, and a granite mantle dike from the UAE. We have observed similar xenocryst dates of ~97–99 Ma in gabbro samples from the ophiolite crust [*Rioux et al*., 2012] and hypothesized that they may be related to propagation of younger ophiolite crust into older, pre-existing oceanic lithosphere. A similar process could explain the older date in the V2 gabbro from this study. It is more difficult to explain the xenocrystic grains in the mantle dikes, which did not interact with the ophiolite crust; however, a cm-scale, late trondhjemite dike that cuts the amphibolite in the Sumeini sole locality contained xenocrystic zircon grains with dates of 98.0–96.4 Ma [*Rioux et al*., 2016]. If the felsic mantle dikes formed by melting of amphibolite and metasediment on the top of a subducting slab [*Haase et al*., 2015; *Rollinson*, 2015; *Spencer et al*., 2017], the older zircon grains observed in the felsic mantle dikes could be inherited from these rocks, some of which have been demonstrated to include zircon grains of the appropriate age [*Garber et al*., 2020]. For the samples with a smaller range of zircon

dates, anomalous grains that are tens to hundreds of thousands of years older than the youngest population may have assimilated from older parts of the magmatic system, assimilated from older wallrocks, or been inherited from the source rocks for the mantle dikes.

The new high-precision dates are younger than the results from two previous laser ablation studies. Tsuchiya et al. [2013] previously reported LA-ICP-MS zircon dates of 99–100 Ma (± 1–2 Ma) from three quartz diorite samples from the early and late intrusive series in the Lasail plutonic complex. In comparison, the quartz diorite we dated from this area yielded a $^{206}Pb/^{238}U$ date of 95.336 ± 0.044 Ma. Similarly, Spencer et al. [2017] dated five felsic mantle dikes from Oman by LA-ICP-MS and reported a weighted mean $^{206}Pb/^{238}U$ date of 99.8 ± 3.3 Ma, again older than the dates of 95.478 ± 0.032 to 94.95 ± 0.10 Ma that we found for the felsic mantle dikes in this study. The Tsuchiya et al. [2013] and Spencer et al. [2017] dates are older than any of the ID-TIMS dates from the ophiolite and we attribute them to systematic biases in the LA-ICP-MS analyses.

6.2 Tectonic evolution of the ophiolite

The U-Pb zircon dataset presented herein supports the formation of the ophiolite during subduction initiation. Models for ophiolite formation through subduction initiation are motivated by similarity in the stratigraphy and chemical evolution of igneous rocks in the forearc of the Izu-Bonin-Mariana (IBM) arc system—which are interpreted to have formed during arc initiation at 52–48 Ma—and some ophiolite lava sequences [e.g., *Ishizuka et al*., 2014; *Ishizuka et al*., 2011; *Reagan et al*., 2010; *Reagan et al*., 2017; *Stern and Bloomer*, 1992]. In the IBM forearc, voluminous early forearc basalts have similar compositions to MORB and are attributed to spreading and decompression melting during the early (<1.2 Ma) stages of subduction initiation [*Reagan et al*., 2019; *Reagan et al*., 2010]. These are overlain by boninitic (high Si, Mg; low Ca, Al; large ion lithophile element, LILE enriched) lavas attributed to shallow, hydrous melting of depleted mantle harzburgites [*Reagan et al*., 2010; *Stern et al*., 2012]. Previous studies have argued that the Samail ophiolite formed during subduction initiation based on the similar geochemical progression from MORB-like V1 lavas to depleted arc tholeiites and boninites in the V2 lavas [*Belgrano and Diamond*, 2019; *Ishikawa et al*., 2002; *Ishizuka et al*., 2014; *Kusano et al*., 2014; *MacLeod et al*., 2013; *Stern et al*., 2012; *Whattam and Stern*, 2011] and evidence of a subduction signature in podiform chromitites in the mantle [*Rollinson and Adetunji*, 2013]; Belgrano and Diamond [2019] and Belgrano et al. [2019] note that there are chemical differences between the IBM forearc basalts and Samail V1 lavas, while arguing the overall similarities between the IBM forearc and Samail section suggest both sections formed in a proto-arc setting.

We propose the following model for the formation of the ophiolite through subduction initiation, based on the chronology established by the U-Pb zircon dates (Figure 7):

1. **Pre-96.2 Ma**: Prior to 96.2 Ma, subduction initiated along a pre-existing weakness in the oceanic lithosphere [e.g., *Stern*, 2004; *Stern and Bloomer*, 1992]. U-Pb dates from the Sumeini metamorphic sole exposure (96.2 Ma) are synchronous with or slightly predate V1 magmatism within the ophiolite, indicating that a subducting plate existed by the time of ophiolite formation [*Rioux et al*., 2016]. This observation, together with the geochemistry of the V1 lavas, is inconsistent with models of ophiolite formation at a ridge-axis followed by subsequent thrusting. Guilmette et al. [2018] recently published Lu-Hf garnet-whole rock isochron dates of ~104–103 Ma (n = 3) from the Wadi Tayin and Sumeini sole localities, and attributed the dates to early thrusting during induced subduction initiation. These dates are older than any existing U-Pb dates from the ophiolite sole and ongoing research seeks to better understand

the offset between the Lu-Hf and U-Pb dates; however, the new garnet dates raise the possibility that sole metamorphism could significantly pre-date formation of the ophiolite crust.

2. **96.1–95.6 Ma:** As subduction developed—potentially reflecting progressive strain localization along the plate interface as a result of cooling and fluid release [*Agard et al.*, 2020]—sinking or rollback of the slab into the mantle led to extension in the over-riding plate and formation of the ophiolite crust through V1 magmatism (96.1–95.6 Ma). Greater than 2 GPa (> 60 km) of decompression melting are required to produce the MORB-like V1 lavas that formed most of the crust [e.g., *Asimow et al.*, 2004; *Kinzler*, 1997; *Kinzler and Grove*, 1992]. While metamorphism in the sole was synchronous with or slightly pre-dated V1-magmatism (~96.15 Ma), we note that peak sole pressures of 1.0 to 1.3 GPa, corresponding to depths of ~30 to 40 km [*Cowan et al.*, 2014; *Soret et al.*, 2017], indicate that metamorphism of the currently preserved sole occurred beneath the forearc, trenchward of the spreading ridge that formed the crust (Figure 7). The 2 GPa melt column for the V1 lavas suggests either a deep slab (>60 km) below the ophiolite—as suggested by the presence of subduction-related major and trace element signatures in the V1 lavas [*MacLeod et al.*, 2013; *Pearce et al.*, 1981]—or that the slab did not yet fully extend below the ophiolite during V1 magmatism [e.g., *Agard et al.*, 2020; *Maunder et al.*, 2020]

   The offset between subduction initiation and initial V1 magmatism is poorly constrained. The currently preserved sole may not have formed during the earliest phases of subduction initiation; *PT* conditions preserved in the sole likely occurred at the top of the subducting slab both prior to and during V1 magmatism, and any record of the earliest phase of subduction initiation may have been subducted or may not be currently exposed. As a result, the offset between the timing of sole metamorphism and V1 magmatism represents a minimum offset between the initiation of subduction and formation of the ophiolite crust. If our previous U-Pb dates from the Sumeini sole locality reflect prograde or peak metamorphism at 96.2 Ma [*Rioux et al.*, 2016], this would suggest a minimum offset of 100–500 ka between subduction initiation and V1 magmatism, whereas the Guilmette et al. [2018] garnet dates would suggest a minimum offset of >7 Ma.
3. **95.6–95.2 Ma:** As the subduction zone matured, release of slab-derived fluids [*Prigent et al.*, 2018b; *Prigent et al.*, 2018c], melts or supercritical liquids led to flux melting of the wedge and early V2 magmatism.
4. **95.2–95.0 Ma**: From 95.2–95.0 Ma, felsic dikes intruded the uppermost mantle and lower crust along the length of the ophiolite in Oman. The negative $\varepsilon_{Nd}(t)$ and trace element signatures of the dikes indicate they formed by melting of metasediments and amphibolite at the top of the subducting slab, with some contributions from mantle-derived magmas or assimilation of mantle harzburgite [*Amri et al.*, 2007; *Haase et al.*, 2015; *Rioux et al.*, in review; *Rollinson*, 2015; *Spencer et al.*, 2017]. The 95.2–95.0 Ma dates overlap with or are younger than the youngest V2 magmatism. Isotopic data from the V2 lavas series show a progression from MORB-like values in the lower V2 magmas ($\varepsilon_{Nd}(t) \sim +8$) to more enriched values in the upper V2 lavas ($\varepsilon_{Nd}(t) = +0.88–5.69$) [*Kusano et al.*, 2017], which is interpreted to reflect a sediment component in the younger V2 lavas. Taken together, the young dates for the felsic mantle dikes—reflecting three-component mixing between amphibolite and sediment melts on the subducted slab and a mantle component [*Haase et al.*, 2015; *Rioux et al.*, in review; *Rollinson*, 2015]—and the enriched isotopic signature of the upper V2 lavas suggest an increasing

proportion of slab melts through time, reflecting either the arrival of subducted terrigenous sediment below the ophiolite or the onset of slab melting [*Maunder et al*., 2020].

5. **Post-95.0 Ma:** The dearth of U-Pb dates younger than 95.0 Ma in the Oman section of the ophiolite, and the absence of evidence for development of a mature volcanic arc, suggest that magmatism in the ophiolite ended abruptly at this time.

We envision two possible geometries for the developing subduction system (Figure 7):

Model 1: The geochemical evolution reflects the maturation and evolution of the subducted slab. In this model, the slab was present below the ridge axis throughout the formation of the ophiolite crust. The V1 lavas formed by decompression mantle melting similar to modern ridges, requiring a >60 km melt column. The geochemistry of the V1 lavas suggest a slab component was added to the melts [*MacLeod et al*., 2013; *Pearce et al*., 1981]. In particular, when data are normalized to Y or Yb to remove the effects of crystal fractionation, V1 lavas have elevated Th and U compared to Nb and Ta, similar to arc magmas. The absence of a strong "continental" isotope signature may indicate that subducted terrigenous sediments and continental crust had not yet reached depths below the spreading axis. Instead, input of a Th- and U-enriched fluid, melt or supercritical liquid component from the subducting oceanic plate impacted the melt trace element signature, but did not contribute an isotopically identifiable component. The development of a more distinctive "arc signature"—still with MORB-like $\varepsilon_{Nd}(t)$—in the lower V2 lavas, could reflect the increasing importance of H_2O-fluxed melting in the evolving mantle wedge above the subduction zone and below the spreading center. The close spatial association of the V1 and V2 lavas indicate the V2 lavas erupted directly over the V1 series [e.g., *Alabaster et al*., 1982; *Belgrano et al*., 2019; *Ernewein et al*., 1988], but the main axis of each series may have been offset and migrated through time, as suggested by geodynamic modeling [e.g., *Leng et al*., 2012; *Maunder et al*., 2020].

Finally, the eruption of boninitic lavas, the shift to less radiogenic $\varepsilon_{Nd}(t)$ in the upper V2 lavas, and intrusion of the low $\varepsilon_{Nd}(t)$ felsic mantle dikes, could be related to i) changing subduction parameters, where sediments were scrapped off during initial penetration of the slab, but a larger volume of sediment was carried down as subduction became established [e.g., *Agard et al*., 2020; *Agard et al*., 2016], ii) a progressive increase in the volume of sediment on the subducting plate [*Garber et al*., 2020], or iii) the onset of slab melting [*Maunder et al*., 2020]. The geochemistry of the felsic mantle dikes suggests melting of the slab surface at <40–45 km [*Rioux et al*., in review], indicating significant shallowing of the slab or offset of the ophiolite toward the trench following eruption of the V1 lavas. In this model, the shallowing of the slab and the abrupt termination of magmatism at 95.0 Ma may reflect initial emplacement of the ophiolite.

Model 2: The temporal evolution of the ophiolite could alternately reflect the progressive penetration of the slab, where V1 lavas were erupted as the slab began sinking, but was not yet directly below the spreading axis [*Maunder et al*., 2020]. This model would imply that the "subduction signature" in the V1 lavas was transported laterally from the nascent slab—perhaps analogous to the observed slab signature in lavas from the South Chile Ridge adjacent to the Chile Trench [e.g., *Karsten et al*., 1996; *Klein and Karsten*, 1995]. The progressive development of V2 magmatism and then intrusion of the felsic mantle dikes could reflect arrival of the subducted slab below the ridge axis. In this geometry, the initial MOR melt column does not

occur above the slab, and as a result, no shallowing of the slab is required prior to intrusion of the felsic mantle dikes (i.e., the slab could arrive below the ridge axis at ~40 km depth). The termination of ophiolite magmatism could reflect truncation of the decompression- or flux-melting column by arrival of the subducted plate below the paleo-ridge axis. The geometry of this model is similar to geodynamic models of subduction initiation by Maunder et al. [2020].

Early establishment of a subducted slab in Model 1 provides a simple explanation of both a slab signature in the V1 lavas [*MacLeod et al*., 2013; *Pearce et al*., 1981] and early metamorphism (>96.2 Ma) within the downgoing plate; however, the model requires shallowing of the slab or movement of the new ophiolite crust toward the trench after V1 magmatism, but prior to slab melting to form the felsic mantle dikes. Model 2 provides simple explanations for the depth of melting for the felsic mantle dikes and the termination of ophiolite magmatism; however, the subduction signature in the V1 lavas then requires lateral transport of slab fluids within the developing mantle wedge and it is more difficult to explain early sole metamorphism if slab development was synchronous with the formation of the ophiolite crust, potentially requiring some crustal thickening prior to subduction initiation (Figure 7) [*Guilmette et al*., 2018]. We currently favor Model 1, which we feel more simply explains the current data, especially subduction-related major and trace element signatures in the V1 lavas [*MacLeod et al*., 2013; *Pearce et al*., 1981].

In either model, rapid cooling of the metamorphic sole following the termination of magmatism suggest emplacement either caused or quickly followed this magmatic shutdown: $^{40}Ar/^{39}Ar$ cooling dates from the metamorphic sole, which record cooling below ~600 ºC, are nearly synchronous within analytical uncertainty to U-Pb zircon crystallization ages for the crustal gabbros [*Hacker et al*., 1996]. The sudden emplacement of the ophiolite could be related to a change in tectonic parameters [*Agard et al*., 2007] or subduction of more buoyant crust, such as younger lithosphere or thickened crust (e.g. sea mounts or the continental margin).

In contrast to the Oman mantle dikes, the UAE mantle dikes significantly post-date formation of the ophiolite crust, with a broad range of dates from 94.1–91.0 Ma. U-Pb dates from the V1 and V2 magmatic series in the UAE are coeval with magmatism in Oman (Figure 5), indicating that crustal magmatism was synchronous along the entire length of the ophiolite and terminated at the same time. In contrast to Oman, the UAE portion of the ophiolite includes the Bani Hamid thrust sheet, which consists of a 1.2 km thick sequences of amphibolite to granulate facies marble, quartzite, calc-silicate, and minor amphibolite [*Searle et al*., 2015]. The Bani Hamid rocks have peak P-T conditions of 850 ± 60 ºC and 0.63 ± 0.05 GPa, recording lower peak pressures than recorded in the metamorphic sole of the ophiolite. The top and bottom of the sheet are in thrust contact with mantle peridotite. The overlap of dates between the Bani Hamid thrust sheet and the adjacent Wadi Hulw bin Sulayman dike suite suggesting a genetic link, as discussed above [*Cox et al*., 1999]. Underplating and thickening of continental crust may have resulted in intrusion of the S-type andalusite-cordierite-garnet dikes, and the folding, thrusting, thickening, and metamorphism of the Bani Hamid granulites below the already obducted ophiolite. Together, the Bani Hamid metamorphism and the late, felsic mantle dikes require the heterogeneous preservation of heat for several million years after most ophiolite magmatism ceased.

The distinct tectonic histories of the Oman and UAE portions of the ophiolite may reflect the geometry and structure of the subducting plate and/or Arabian continental margin, or the geometry of the nascent subduction zone. With respect to the latter, van Hinsbergen et al. [2019] recently proposed that the Samail ophiolite formed during subduction initiation along a NNE-SSW oriented fracture zone, oriented perpendicular to the Arabian margin. In this model, the ophiolite

then rotates around an Euler pole at the northern end of the ophiolite (present geographical reference frame), eventually being obducted onto the Arabian margin. This type of differential rotation could have implications for the thermal structure and composition of the subducted material along the length of the ophiolite. If the rotation axis is close to the modern northern end of the ophiolite, rotation would lead to more rapid subduction—and likely cooling of the subduction zone—in the south. A hotter thermal structure in the north could promote prolonged melting of subducted sediment or continental crust, leading to formation of the younger UAE felsic mantle dikes. Differential rotation or the geometry of the Arabian continental margin may also have led to variations in the composition of material being subducted below the ophiolite, and early subduction of a thicker package of terrestrial sediment or continental crust could also explain the formation of the younger UAE felsic mantle dikes. Further research is needed to differentiate between these models and better understand the origin of the younger felsic dikes in the UAE portion of the ophiolite and their implications for the tectonic history of the Samail ophiolite.

While initial emplacement of the ophiolite was likely synchronous with the termination of magmatism in the ophiolite at ~95.0 Ma, we consider it likely that the established subduction zone continued for at least another 15 Ma. Post 95.0 Ma, this subduction consumed the remaining oceanic basin and parts of the Arabian continental margin during obduction of the ophiolite onto the continent [*Searle and Cox*, 1999; *Searle et al*., 1994]. Remnants of the subducted continental margin are preserved as a series of exhumed thrust sheets in the Saih Hatat [*Agard et al*., 2010; *Searle et al*., 1994; *Yamato et al*., 2007], including ultrahigh-pressure eclogites at As Sifah beach, on the north-east coast of Oman, which record metamorphic U-Pb dates of ~80 Ma [*Searle et al*., 1994; *Warren et al*., 2005; *Warren et al*., 2003]. Subduction of the thick, buoyant Arabian continental margin may have eventually clogged the subduction zone, leading to slab breakoff and exhumation of the As Sifah UHP rocks up the subduction channel [*Agard et al*., 2010; *Searle et al*., 2004].

An outstanding issue in the Samail ophiolite is the absence of evidence of a mature volcanic arc, despite active subduction for more than 15 Ma. Our work does not directly address this issue; however, the absence of an arc could be related to subduction of buoyant crust during initial emplacement of the ophiolite and the subsequent underthrusting of the continental margin. In a careful study, Bonnet et al. [2020] document evidence of a subducted seamount, now exposed in the Zagros Mountains, which records a transition from subduction-related to mid-ocean ridge magmatism from 87–78 Ma. The authors propose the seamount could be from a remnant arc related to the evolution of the Samail ophiolite, with arc magmatism shifting away from the trench after formation of the ophiolite. However, sediments overlying the ophiolite volcanic sequence do not contain tephra layers [*Ernewein et al*., 1988; *Fleet and Robertson*, 1980; *Hara and Kurihara*, 2017], suggesting any arc magmatism was limited in scope. In comparison, sediments in the IBM forearc contain abundant tephra layers [*Kutterolf et al*., 2018; *Robertson et al*., 2018], reflecting the formation of a mature arc; there is a 15 Ma hiatus in the IBM forearc between the end of forearc volcanism and the oldest preserved sediments, but fossil ages indicate a similar hiatus does not exist in Oman [*Hara and Kurihara*, 2017; *Tippit et al*., 1981] and the sedimentary section would likely record evidence of any proximal arc volcanism.

6.3 Comparison to the Izu-Bonin-Mariana forearc

The existing data from the Samail ophiolite and new data presented here allow for comparison of the geochemical and temporal evolution of the ophiolite and the record of subduction initiation in the IBM forearc. Belgrano et al. [2019] recently published a comparison of trace element data from

the two localities. They note differences in the trace element compositions of the Samail and IBM forearc lavas—including higher Ti/V in Samail V1 versus IBM forearc basalts and elevated Zr in IBM boninites—which they argue may be related to prior depletion of the mantle wedge in the IBM and differences in the composition of subducted crust. Overall, they conclude that the similar structure and progressive depletion trends for the two localities support formation of the Samail ophiolite during subduction initiation. In another recent contribution, Li et al. (2019) present radiogenic isotope data (Hf, Nd, Sr, Pb) from forearc basalt and boninite samples recovered from the IBM forearc during International Ocean Discovery Program (IODP) Expedition 352. They document a progressive shift from higher ε_{Nd}, ε_{Hf}, and lower $^{87}Sr/^{86}Sr$ in forearc basalts to lower ε_{Nd}, ε_{Hf}, and higher $^{87}Sr/^{86}Sr$ in boninitic samples, which they attribute to incorporation of a larger slab component—including amphibolite and sediment melts—in the boninitic lavas. The observed progression is similar to the isotopic record of the Oman ophiolite from high ε_{Nd} and ε_{Hf} in the V1 and lower V2 lavas to less radiogenic compositions in the upper V2 lavas [*Amri et al*., 2007; *Godard et al*., 2006; *Haase et al*., 2015; *McCulloch et al*., 1981; *Rioux et al*., 2012; *Rioux et al*., 2013; *Tsuchiya et al*., 2013] and the late felsic mantle dikes [this study; *Amri et al*., 2007; *Briqueu et al*., 1991; *Cox et al*., 1999; *Haase et al*., 2015; *Lippard et al*., 1986; *Rioux et al*., 2013]. The magnitude of the shift is much smaller in the IBM— IBM lavas range from ε_{Nd} = 9.7 to 6.8, while the Samail V1 and V2 range from ε_{Nd} = 9.1 to 0.7—which may again reflect differences in the composition of the subducted slab.

Our U-Pb data indicate that temporal evolution of the Samail ophiolite is also similar to the duration of pre-arc magmatism in the IBM forearc. Ishizuka et al. [2011] used $^{40}Ar/^{39}Ar$ and secondary ion mass spectrometry (SIMS) U-Pb dating of marine and subaerial samples from the Bonin Ridge and Bonin Islands to study the temporal evolution from early forearc basalts and related gabbros, to boninitic volcanism. They found that studied forearc basalts and gabbros erupted from 52–48 Ma, followed by a transition to boninitic volcanism from 48–44 Ma, suggesting a 2–4 Ma transition from MORB-like compositions to a subduction signature. More recently, Reagan et al. [2019] carried out a detailed study of the forearc basalt to boninitic transition in the Bonin forearc. They reported high-precision U-Pb zircon and $^{40}Ar/^{39}Ar$ dates from samples collected by submersible (Shinkai 6500 Dive 6K1149) and drilling (IODP Holes U1439–U1442) over a ~24 km transect, roughly orthogonal to the trench. A gabbro and basalt, both related to initial spreading and forearc basalt magmatism, yielded dates of 51.94 ± 0.15 and 51.34 ± 0.78 Ma, respectively. This was followed by boninitic volcanism from >51.27 ± 0.09 to 50.33 ± 0.55 Ma. A regression of the data suggests a total duration of spreading of 0.6–2 Ma and that the progression from subduction initiation and the eruption of forearc basalts to the development of a subduction zone signature occurred over <1.2 Ma [*Reagan et al*., 2019]. These timescales are similar to our data from Oman, where V1 volcanism lasted for ~0.5 Ma (96.1–95.6 Ma) and was followed by 0.4 Ma of V2 magmatism (95.6–95.2 Ma).

6.4 Comparison to geodynamic models

If the Samail ophiolite formed during subduction initiation, as we propose, the temporal evolution of magmatism within the ophiolite can also be compared to geodynamic models of this process [e.g., *Dymkova and Gerya*, 2013; *Gerya et al*., 2008; *Gurnis et al*., 2004; *Hall et al*., 2003; *Leng and Gurnis*, 2011]. The models of Leng et al. [2012] are particularly useful, because they link the geodynamic modeling with melting parameterizations, to predict the composition and duration of melting during subduction initiation. Model parameters that account for the release of water from the slab into the mantle wedge and lead to subduction initiation with forearc spreading and no slab

breakoff (Figures 3 and 5 of Leng et al., 2012), predict a volcanic progression similar to the IBM forearc and the Samail ophiolite, from MORB-like basalts to more boninitic compositions. The Leng et al. [2012] models used forced subduction initiation—where a constant convergence rate leads to development of subduction—but the authors suggest that after initial foundering of the slab, the conditions are similar to models of spontaneous subduction initiation due to gravitational instability. For model A01, following ~ 4.2 Ma of initial convergence, the melting model predicts 0.5–1 Ma of MORB-like basalt eruptions (position 500–525 km) followed by a transition to more depleted magmas with an increasingly evident subduction signature, and ultimately boninitic volcanism (subducting plate age = 82 Ma, imposed velocity= 4.0 cm/yr). These timescales are similar to the 0.5 Ma of V1 magmatism in the Samail ophiolite, prior to appearance of the subduction related V2 magmatism. The magmatic evolution is dependent on the applied model parameters, and models with varying subducting plate ages (42 to 82 Ma) and imposed velocities (2.0–4.0 cm/yr) show variable durations of MORB-like magmatism from 0.25–2.25 Ma. The timescales of the Leng et al. [2012] models are therefore broadly consistent with the duration of magmatism in the Samail ophiolite, though they depend on the chosen model parameters.

Modeling by Maunder et al. [2020] focused specifically on reproducing the geology and geochemistry of the IBM forearc, again combining numerical modeling with melt parameterization. These authors suggest that subduction initiation in the IBM system is best explained by "vertically driven" initiation, referring to a mechanism dominated by vertical buoyancy forces, similar to spontaneous initiation models from previous studies. The Maunder et al. [2020] models predict a progression following subduction initiation of forearc basalt volcanism from 60–630 ky, hydrous boninites from 630–830 ky, and the onset of slab melting at 830 ky. The temporal evolution is strikingly similar to the progression in the Semail ophiolite of V1 magmatism from 96.1–95.6 Ma (0–500 ka), V2 magmatism related to H_2O-fluxed mantle melting from 95.6–95.2 (500–900 ka) Ma, and intrusion of felsic dikes within the mantle (likely reflecting slab meting) from 95.2–95.0 Ma (900–1100 ka after the earliest V1 magmatism). However, the geometries of the vertically driven initiation models appear to be at odds with the U-Pb dates from the Samail metamorphic sole, which suggest initial sole metamorphism was coeval with or slightly pre-dates ophiolite spreading (~96.2 Ma), suggesting that the subducted slab was at depths of 30–40 km (assuming minimal overpressure) [e.g., *Garber et al*., 2020]. In contrast, in the Maunder et al. [2020] models, most spreading related magmatism (forearc basalt or V1) occurs before significant sinking of the downgoing slab. Early sole metamorphism may instead reflect induced subduction initiation [*Guilmette et al*., 2018].

It is more difficult to infer the geochemical evolution of volcanism from other studies; however, in general, the short duration of magmatism in Oman is consistent with many of the published geodynamic models. In a review paper, Gerya [2011] noted that numerical models of spontaneous subduction initiation along existing zones of weakness in several studies predict rapid extension in the over-riding plate, likely leading to the eruption of boninites and the formation of ophiolites in the initial 0.3–1.5 Ma [*Gerya*, 2011; *Gerya et al*., 2008; *Nikolaeva et al*., 2008; *Zhu et al*., 2009]. Duretz et al. [2016] presented a 2-D thermo-mechanical model focused on recreating the tectonic history of the Samail ophiolite. In their model, conditions consistent with the peak *P-T* of the metamorphic sole develop in the downgoing plate within 1.5 Ma, and the ophiolite is obducted onto the continent about 4 Ma after subduction initiation, again suggesting rapid formation of the ophiolite crust together with a transition to V2 magmatism.

6.5 Formation and preservation of the felsic mantle dikes

The felsic mantle dikes from the Oman portion of the ophiolite yielded dates of 95.5–95.0 Ma. As outlined above, we attribute the six youngest dikes (92.2–95.0 Ma) to melting of sediment and amphibolite on top of a subducting plate [*Haase et al*., 2015; *Pearce*, 1989; *Rioux et al*., 2013; *Rollinson*, 2009; *Rollinson*, 2014; 2015; *Spencer et al*., 2017], while the older dike (13217M01; 95.5 Ma) may be related to V2 magmatism. Geodynamic models of subduction initiation predict melting at the top of a foundering slab under a range of model parameters [*Maunder et al*., 2020; *Nikolaeva et al*., 2008] and the composition of the felsic dikes is consistent with melting of the amphibolite and metasedimentary lithologies exposed below the ophiolite [*Rollinson*, 2015], including metasediments and leucocratic pods within the sole with negative $\varepsilon_{Nd}(t)$ [*Rioux et al*., 2013; *Rioux et al*., 2016].

Taken together, the peak *P-T* estimates for the metamorphic sole, the formation of the mantle dikes by melting of subducted material, the crystallization of these dikes within the uppermost mantle and the coeval V2 boninite volcanism, all suggest steep thermal gradients within the nascent subduction zone. The boninite lavas occur in the upper portions of the V2 lava series, which our dating suggests is coeval with or immediately pre-dates crystallization of the felsic mantle dikes. Experiments demonstrate that the formation of boninites requires high temperature, low pressure melting (1250 to >1400 ºC, ≤30 to 45 km), suggesting a hot mantle wedge at this time [*Falloon and Danyushevsky*, 2000; *Ishikawa et al*., 2002]. Metamorphic conditions in the sole are hotter than typical subduction zone geotherms, consistent with a hot, shallow mantle wedge [*Cowan et al*., 2014; *Peacock*, 1991; *Peacock*, 1996; *Soret et al*., 2017; *Syracuse et al*., 2010]. Such high slab temperatures are required if the dikes are derived from sub-ridge melting of lithologies similar to those found in the sole. Experiments on fluid-present melting of amphibolite and metasediment at pressures of 1–5 GPa record solidus temperatures of 700–900ºC [e.g., *Kessel et al*., 2005; *Moyen and Stevens*, 2006; *Schmidt et al*., 2004], consistent with pseudosection modeling for sole amphibolites [*Soret et al*., 2017].

In contrast to the evidence of high temperatures at the top of the subducted plate and within the overlying mantle wedge, crystallization of the felsic dikes near the crust-mantle boundary indicate that the uppermost mantle had cooled below the solidus temperature of the dikes prior to intrusion at 95.5–95.0 Ma (~600–700 ºC) [*Huang and Wyllie*, 1975; *Huang and Wyllie*, 1981]. Rapid cooling of the uppermost mantle is consistent with evidence for deep hydrothermal circulation to near Moho depths close to the ridge axis in the Samail ophiolite [*Dygert et al*., 2017; *Hanghøj et al*., 2010; *VanTongeren et al*., 2008]. The formation and crystallization of the felsic mantle dikes and the synchronous or near synchronous eruption of boninites within the V2 lavas therefore suggest a steep vertical thermal gradient between hydrothermally cooled uppermost mantle, the hot core of the mantle wedge, and the hot subduction zone beneath the spreading ridge.

An important consideration is how the felsic dikes were able to traverse the hot mantle wedge. Given the large chemical and thermal gradients between the dikes and mantle peridotite, it is expected that the dikes would have been heated to superliquidus temperatures and reacted with the surrounding peridotite [*Kelemen*, 1986; *Kelemen*, 1990; *Kelemen and Ghiorso*, 1986; *Rapp et al*., 2010; *Sen and Dunn*, 1995]. This may have led to melt-fluxed melting [*Grove et al*., 2012; *Kelemen et al*., 2003], potentially contributing to the V2 geochemical signature [*Haase et al*., 2015; *Kusano et al*., 2017], as suggest by the lower $\varepsilon_{Nd}(t)$ (+0.88 to +5.69) from upper V2 lavas (Figure 6) [*Kusano et al*., 2017]. Pearce et al. [1992] noted evidence for a similar amphibolite melt component in the trace element composition of boninites formed during subduction initiation in the Izu-Bonin arc.

However, while we consider it likely that slab melts contributed to melt-flux melting, the preserved felsic mantle dikes show that some slab melts successfully traversed the wedge, with little chemical interaction with the surrounding peridotite, as previously suggested by oxygen isotope analyses [*Spencer et al*., 2017]. The Ni and MgO content of the felsic mantle dikes can be used as a proxy for the degree of mantle reaction; sediment ± amphibolite melts are expected to have low Ni and MgO and concentrations of these elements will increase as a result of interaction with or assimilation of olivine and orthopyroxene from peridotite [*Kelemen et al*., 1998]. Ni and MgO concentrations in the dikes are variable, with dikes from the Haylayn block defining a mixing trend to a high Ni, high MgO end member, interpreted to be either basaltic melts [*Haase et al*., 2015] or mantle peridotite [*Rollinson*, 2015]. In contrast, the dated dikes from the Fizh, Bahla and Wadi Tayin massifs (13215M08, 13211M02, 13221M05) have low Ni (1.5–4.4 ppm) and MgO (0.1–0.6 wt. %) [*Rioux et al*., in review], suggesting minimal reaction with mantle peridotite.

The preserved dikes may have been able to rapidly traverse the hot wedge due to the development of thermo-chemical plumes, sediment diapirism or reactive armoring. Numerical modeling predicts that slab dehydration and wedge melting can lead to the formation of cooler thermo-chemical plumes (ΔT = 100–300 ºC) that propagate into the mantle wedge above subducting plates [*Gorczyk et al*., 2007; *Zhu et al*., 2009]. Alternately, Behn et al. (2011) demonstrated that subducted sediment may detach from the down-going plate and rise as diapirs into the mantle wedge. Finally, observations of felsic melts within mantle peridotite xenoliths document the development of pyroxene reaction zones around intrusions, which once established, could shield slab melts from extensive reaction with the hot core of the mantle wedge [*Arai et al*., 2003; *Myers et al*., 1985; *Shimizu et al*., 2004]. Reaction rims are not observed around the preserved dikes that crystallized within the cool upper mantle and we are not aware of any evidence for sediment plumes in the ophiolite mantle section, but it is possible one or both features formed in higher temperature portions of the mantle at depth.

The geochemistry of the dikes also suggest emplacement through a thin mantle wedge [*Rioux et al*., in review]. If the slab was present below the ridge during V1 magmatism (>60 km depth; Figure 7, Model 1), it would have had to shallow significantly prior to formation of the felsic dikes (~40–45 km), as discussed for Model 1 (progressive thinning of the wedge is not required for Model 2). Thinning of the wedge, if it did occur, could reflect shallowing of the subducting plate perhaps due to the subduction of progressively more buoyant material approaching the continental margin, movement of the ophiolite crust toward the trench during the first stages of obduction, or other processes [e.g., tectonic thinning: *Agard et al., 2020; Prigent et al., 2018a*; or magmatic thinning: *van Hinsbergen et al., 2015*]. Intrusion of the felsic mantle dikes from ~95.2–95.0 Ma, may therefore reflect thinning of the wedge and the development of channels over time, which provided a path for the felsic mantle dikes to reach the cool upper mantle.

In contrast to the above discussion, Haase et al. [2015] proposed that the dikes may instead have intruded through the cool, serpentinized tip of the wedge. If this model is correct, it would require rapid cooling of the wedge between the eruption of V2 boninites and emplacement of the dikes or thrusting of the ophiolite towards the cooler tip of the wedge. The dikes and V2 lavas occur within the same ophiolite massifs, precluding a significant spatial offset. The U-Pb dates for the dikes overlap with, or are only ≤200 ka younger than, the V2 magmatism, and as such, could be consistent with very rapid cooling. The presence of inherited zircon grains in some of the mantle dikes could also support a cooler wedge model; zircon will dissolve rapidly in anatectic melts of amphibolite and metasediment above temperatures of ~1000 °C [e.g., *Watson and Harrison*, 1983] and the preservation of inherited grains suggests that the magmas that formed the mantle dikes

traversed the wedge without significant heating, either in large diapirs moving so rapidly that they did not thermally equilibrate with their surroundings, or after cooling of the mantle wedge from the high temperatures required for boninite formation. However, we consider the cool wedge model to be less likely because i) our data suggest a very limited time gap between V2 magmatism and the crystallization of the mantle dikes, and ii) the amphibolite and sediment at the top of the subducting plate would have been unlikely to reach solidus temperatures below the cooler serpentinized nose of the wedge.

7. Conclusions

New and existing high-precision U-Pb zircon dates constrain the tectonic evolution of the Samail ophiolite. The data are consistent with formation during subduction initiation. In this context, we reconstruct the following sequence of events: 1. Subduction initiated prior to 96.2 Ma, with initial metamorphism in the metamorphic sole slightly predating ophiolite formation; 2. The main portion of the ophiolite crust formed due to decompression melting of the mantle—with minor input from a slab component—driven by spreading in the overriding plate as a result of slab rollback from 96.1–95.6 Ma (V1); 3. An increasingly important component of H_2O-fluxed melting, driven by production of hydrous fluids, melts or supercritical liquids from altered basalts in the subducting plate led to formation of the V2 magmatic series from 95.6–95.2 Ma; 4. Toward the end of V2 magmatism, felsic dikes—formed by three component mixing between metasediment and amphibolite melts of the top of the subducting slab and a mantle component—crystallized within the uppermost mantle from 95.2–95.0 Ma. These data suggest either the progressive thinning of the Samail mantle wedge during ophiolite development, or alternatively the progressive arrival of the tip of a subducted slab beneath the ophiolite. Younger felsic mantle dikes in the northernmost ophiolite exposures (UAE; 94.1–91.0 Ma) likely reflect along strike differences in the rate of subduction or the composition of subducted material. The duration of the V1 and V2 magmatism in the ophiolite is similar to the temporal development of magmatism in geodynamic models of subduction initiation and recent geochronologic constraints on crustal growth during subduction initiation in the IBM forearc.

Acknowledgements:

This research was supported by United States National Science Foundation grants EAR-1250522 and 1650407 to Matthew Rioux. We thank Georges Ceuleneer and Mathieu Benoit for sharing the location of mantle dikes with us and discussion of the data. We are grateful to Adolphe Nicolas and Françoise Boudier for their help in the field and for many discussions of Oman geology both in the field and over e-mail. We thank the Public Authority for Mining for their support of our research in the Sultanate of Oman, and Mohammed Ali and Aisha Al Suwaidi at Khalifa University for all their help during our field work in the United Arab Emirates. We thank Mathieu Soret, Christopher Spencer, and Editor Steve Parman for their detailed reviews, which substantially improved this manuscript. Josh Garber acknowledges support from National Science Foundation grant OISE-1545903 and The Pennsylvania State University. Reported whole rock isotope data are available through the EarthChem Library (https://doi.org/10.26022/IEDA/111897) and the U-Pb zircon data are available through both the EarthChem Library (https://doi.org/10.26022/IEDA/111910) and the Geochron database (www.geochron.org).

Figure Captions

Figure 1. Geologic map of the Samail (Oman-United Arab Emirates) ophiolite. Inset shows a location map. Dated samples from this study, Rioux et al. [2012; 2013; 2016] and Searle et al. [2015]; samples from this study are distinguished by larger plot symbols with bold sample numbers. Red open rectangles show the locations of Figures 2a–d (Fig. 2a outline is exaggerated for visibility). Blue stars mark the Wadi Tayin (WT) and Sumeini (SUM) sole localities. Massif names are in italics. Map after Nicolas et al. [2000].

Figure 2. (a–d) Geologic maps of the Lasail, Aswad, Wadi Rajmi, and Fizh-South areas, showing the location of V2 plutonic rocks dated in this study (larger yellow squares) and V1 plutonic rocks dated by Rioux et al. [2016] (red squares). Geologic maps are after Adachi and Miyashita [2003], Styles et al. [2006a], Tsuchiya et al. [2013] and Usai and Yamazaki [2010]. Each map is draped over a hillshade derived from the Shuttle Radar Topography Mission (SRTM) 1 Arc-Second Global dataset. Abbreviations are volc., volcanic; sheet. dikes, sheeted dikes; plut., plutonic; gb., gabbro; wehr., wehrlite; Quat. sed., Quaternary sediments; gbn, gabbronorite.

Figure 3. New Th-corrected $^{206}Pb/^{238}U$ dates from V2 plutonic rocks and felsic dikes that intrude mantle harzburgite or the lowest level of the layered gabbros. Each bar corresponds to a single zircon date ± 2σ uncertainties. Reported dates are weighted mean $^{206}Pb/^{238}U$ dates ± 2σ uncertainties, calculated from multiple single zircon analyses; open plot symbols were excluded from the weighted mean calculations. For 13221M05 and M13-1, the reported dates are interpreted crystallization ages based on a single zircon analysis. Imprecise single zircon analyses were excluded from the plots for clarity (2σ ≥ 0.45 Ma; Supplementary Text S1; Supplementary Table S1). Dates are in millions of years (Ma). Arrows denote xenocrystic zircon grains that plot off scale (see Supplementary Figure S2 for concordia plots of the full dataset). MSWD, mean square of the weighted deviates.

Figure 4. Summary of Th-corrected zircon $^{206}Pb/^{238}U$ dates from the Oman portion of the ophiolite from this study (bold sample numbers) and Rioux et al. [2012; 2013; 2016]. Each datum and error bar (± 2σ) correspond to a single zircon analysis and clusters of data are analyses from a single sample. Arrows denote samples with inherited older zircon grains that plot off scale. Dates within each series are arranged from south to north. Imprecise single zircon dates from this study (2σ ≥ ± 0.3 Ma) and our previous research (2σ ≥ ± 0.3 Ma or as described in Rioux et al., 2016) were excluded for clarity. Sample 13217M01 is a felsic dike within the mantle; however, its isotopic and trace element signature suggest it is related to the V2 magmatic series, as discussed in the text. See Supplementary Text S1 for a discussion of the inclusion of samples 8121M05 and 8122M02 in the V2 magmatic series. We exclude samples 8111M02, 8121M04A, and 8122M01 from this plot, which yielded lower precision dates than other nearby samples. Abbreviations are ton., tonalite; trond., trondhjemite. "Sole melts" refer to leucocratic pods within amphibolite in the metamorphic sole.

Figure 5. Summary of Th-corrected zircon $^{206}Pb/^{238}U$ dates from the United Arab Emirates portion of the ophiolite from this study (bold sample numbers), Rioux et al. [2016] and Searle et al. [2015]. Plot parameters are described in the Fig. 3 caption. The diagonally hatched bands show the range of interpreted crystallization ages, excluding uncertainties, for samples in each series in the Oman portion of the ophiolite. The range of dates for the Oman mantle dikes excludes sample 13217M01,

which we attribute to V2 magmatism [*Rioux et al*., in review]. Sample 131213M03 comes from a mapped exposure of V2 plutonic rocks, but the older dates suggest it may actually be a V1 intrusion. Abbreviations are ton., tonalite; trond., trondhjemite; amph., amphibolite.

Figure 6. Summary of Nd isotopic data from the Oman and UAE portions of the Samail ophiolite. Larger plot symbols for the V2 plutonic rocks, felsic mantle dikes and Bani Hamid rocks are data from this study. Smaller symbols in panel (a) are from published datasets [*Amri et al*., 2007; *Briqueu et al*., 1991; *Cox et al*., 1999; *Godard et al*., 2006; *Haase et al*., 2015; *Haase et al*., 2016; *Kusano et al*., 2017; *McCulloch et al*., 1981; *Rioux et al*., 2012; *Rioux et al*., 2013; *Rioux et al*., 2016; *Tsuchiya et al*., 2013]. Smaller symbols in panels (b) and (c) are from our previously published data [*Rioux et al*., 2012; *Rioux et al*., 2013; *Rioux et al*., 2016]. For the sole data, black symbols are from Oman and gray symbols are from the UAE. Upper V2 lavas, with low $\varepsilon_{Nd}(t)$, correspond to the upper V2 unit of Kusano et al. [2017], with the addition of a low $\varepsilon_{Nd}(t)$ from Hilti, which they include in the lower V2 unit. McCulloch et al. [1981] data are recalculated to be consistent with the reduction parameters used in the other studies. All Nd isotopic data are age corrected to 96 Ma.

Figure 7. Tectonic models for formation of the Samail ophiolite during subduction initiation. The temporal evolution is constrained by the U-Pb data present herein and in previous publications [*Rioux et al*., 2012; *Rioux et al*., 2013; *Rioux et al*., 2016]. Litho., lithosphere.

References

Adachi, Y., and S. Miyashita (2003), Geology and petrology of the plutonic complexes in the Wadi Fizh area: Multiple magmatic events and segment structure in the northern Oman ophiolite, *Geochemistry, Geophysics, Geosystems*, *4*(9), 8619.

Agard, P., M. P. Searle, G. I. Alsop, and B. Dubacq (2010), Crustal stacking and expulsion tectonics during continental subduction: P-T deformation constraints from Oman, *Tectonics*, *29*(5).

Agard, P., L. Jolivet, B. Vrielynck, E. Burov, and P. Monié (2007), Plate acceleration: The obduction trigger?, *Earth and Planetary Science Letters*, *258*(3), 428-441.

Agard, P., C. Prigent, M. Soret, B. Dubacq, S. Guillot, and D. Deldicque (2020), Slabitization: Mechanisms controlling subduction development and viscous coupling, *Earth-Science Reviews*, *208*, 103259.

Agard, P., P. Yamato, M. Soret, C. Prigent, S. Guillot, A. Plunder, B. Dubacq, A. Chauvet, and P. Monié (2016), Plate interface rheological switches during subduction infancy: Control on slab penetration and metamorphic sole formation, *Earth and Planetary Science Letters*, *451*, 208-220.

Alabaster, T., J. A. Pearce, and J. Malpas (1982), The volcanic stratigraphy and petrogenesis of the Oman ophiolite complex, *Contributions to Mineralogy and Petrology*, *81*(3), 168-183.

Ambrose, T. K., and M. P. Searle (2019), 3-D Structure of the Northern Oman-UAE Ophiolite: Widespread, Short-Lived, Suprasubduction Zone Magmatism, *Tectonics*, *38*(1), 233-252.

Amri, I., G. Ceuleneer, M. Benoit, M. Python, E. Puga, and K. Targuisti (2007), Genesis of granitoids by interaction between mantle peridotites and hydrothermal fluids in oceanic spreading setting in the Oman ophiolite, *Geogaceta*, *42*, 23-26.

Arai, S., Y. Shimizu, and F. Gervilla (2003), Quartz diorite veins in a peridotite xenolith from Tallante, Spain: implications for reaction and survival of slab-derived SiO₂-

oversaturated melt in the upper mantle, *Proceedings of the Japan Academy, Series B*, *79B*(6), 145-150.
Asimow, P. D., J. E. Dixon, and C. H. Langmuir (2004), A hydrous melting and fractionation model for mid-ocean ridge basalts: Application to the Mid-Atlantic Ridge near the Azores, *Geochemistry, Geophysics, Geosystems*, *5*(1).
Belgrano, T. M., and L. W. Diamond (2019), Subduction-zone contributions to axial volcanism in the Oman–U.A.E. ophiolite, *Lithosphere*, *11*(3), 399-411.
Belgrano, T. M., L. W. Diamond, Y. Vogt, A. R. Biedermann, S. A. Gilgen, and K. Al-Tobi (2019), A revised map of volcanic units in the Oman ophiolite: insights into the architecture of an oceanic proto-arc volcanic sequence, *Solid Earth*, *10*(4), 1181-1217.
Bonnet, G., P. Agard, H. Whitechurch, M. Fournier, S. Angiboust, B. Caron, and J. Omrani (2020), Fossil seamount in southeast Zagros records intraoceanic arc to back-arc transition: New constraints for the evolution of the Neotethys, *Gondwana Research*, *81*, 423-444.
Boudier, F., G. Ceuleneer, and A. Nicolas (1988), Shear zones, thrusts and related magmatism in the Oman ophiolite: Initiation of thrusting on an oceanic ridge, *Tectonophysics*, *151*(1-4), 275-296.
Boudier, F., A. Nicolas, and B. Ildefonse (1996), Magma chambers in the Oman ophiolite: fed from the top and the bottom, *Earth and Planetary Science Letters*, *144*(1–2), 239-250.
Bowring, J. F., N. M. McLean, and S. A. Bowring (2011), Engineering Cyber Infrastructure for U-Pb Geochronology: Tripoli and U-Pb_Redux, *Geochemistry, Geophysics, Geosystems*, doi: 10.1029/2010GC003479.
Briqueu, L., C. Mével, and F. Boudier (1991), Sr, Nd and Pb isotopic constraints on the genesis of a calc-alkaline plutonic suite in the Oman mountains related to the obduction process, in *Ophiolite genesis and evolution of the oceanic lithosphere*, edited by P. Tea, pp. 517–542, Ministry of Petroleum and Minerals, Sultanate of Oman.
Coogan, L. A., G. R. T. Jenkin, and R. N. Wilson (2002), Constraining the cooling rate of the lower oceanic crust: a new approach applied to the Oman ophiolite, *Earth and Planetary Science Letters*, *199*(1-2), 127-146.
Cowan, R. J., M. P. Searle, and D. J. Waters (2014), Structure of the metamorphic sole to the Oman Ophiolite, Sumeini Window and Wadi Tayyin: implications for ophiolite obduction processes, *Geological Society, London, Special Publications*, *392*(1), 155-175.
Cox, J., M. Searle, and R. Pedersen (1999), The petrogenesis of leucogranitic dykes intruding the northern Semail ophiolite, United Arab Emirates: field relationships, geochemistry and Sr/Nd isotope systematics, *Contributions to Mineralogy and Petrology*, *137*(3), 267-287.
Duretz, T., P. Agard, P. Yamato, C. Ducassou, E. B. Burov, and T. V. Gerya (2016), Thermo-mechanical modeling of the obduction process based on the Oman Ophiolite case, *Gondwana Research*, *32*, 1-10.
Dygert, N., P. B. Kelemen, and Y. Liang (2017), Spatial variations in cooling rate in the mantle section of the Samail ophiolite in Oman: Implications for formation of lithosphere at mid-ocean ridges, *Earth and Planetary Science Letters*, *465*, 134-144.
Dymkova, D., and T. Gerya (2013), Porous fluid flow enables oceanic subduction initiation on Earth, *Geophysical Research Letters*, *40*(21), 5671-5676.
Ernewein, M., C. Pflumio, and H. Whitechurch (1988), The death of an accretion zone as evidenced by the magmatic history of the Sumail ophiolite (Oman), *Tectonophysics*, *151*(1-4), 247-274.

Falloon, T. J., and L. V. Danyushevsky (2000), Melting of Refractory Mantle at 1·5, 2 and 2·5 GPa under Anhydrous and H2O-undersaturated Conditions: Implications for the Petrogenesis of High-Ca Boninites and the Influence of Subduction Components on Mantle Melting, *Journal of Petrology*, *41*(2), 257-283.
Fleet, A. J., and A. H. F. Robertson (1980), Ocean-ridge metalliferous and pelagic sediments of the Semail Nappe, Oman, *Journal of the Geological Society*, *137*(4), 403-422.
Garber, J. M., M. Rioux, A. R. C. Kylander-Clark, B. R. Hacker, J. D. Vervoort, and M. P. Searle (2020), Petrochronology of Wadi Tayin Metamorphic Sole Metasediment, With Implications for the Thermal and Tectonic Evolution of the Samail Ophiolite (Oman/UAE), *Tectonics*, *39*(12), e2020TC006135.
Gass, I. G., et al. (1983), Open University Oman Ophiolite Project (Memoir Map), The Open University.
Gerya, T. (2011), Intra-oceanic subduction zones, in *Arc-continent collision*, edited, pp. 23-51, Springer.
Gerya, T. V., J. A. Connolly, and D. A. Yuen (2008), Why is terrestrial subduction one-sided?, *Geology*, *36*(1), 43-46.
Ghent, E. D., and M. Z. Stout (1981), Metamorphism at the Base of the Samail Ophiolite, Southeastern Oman Mountains, *J. Geophys. Res.*, *86*(B4), 2557-2571.
Gnos, E. (1998), Peak Metamorphic Conditions of Garnet Amphibolites Beneath the Semail Ophiolite: Implications for an Inverted Pressure Gradient, *International Geology Review*, *40*(4), 281-304.
Godard, M., D. Bosch, and F. Einaudi (2006), A MORB source for low-Ti magmatism in the Semail ophiolite, *Chemical Geology*, *234*(1-2), 58-78.
Goodenough, K., M. Styles, D. Schofield, R. Thomas, Q. Crowley, R. Lilly, J. McKervey, D. Stephenson, and J. Carney (2010), Architecture of the Oman–UAE ophiolite: Evidence for a multi-phase magmatic history, *Arabian Journal of Geosciences*, *3*(4), 439-458.
Gorczyk, W., T. V. Gerya, J. A. D. Connolly, and D. A. Yuen (2007), Growth and mixing dynamics of mantle wedge plumes, *Geology*, *35*(7), 587-590.
Grove, T. L., C. B. Till, and M. J. Krawczynski (2012), The Role of H2O in Subduction Zone Magmatism, *Annual Review of Earth and Planetary Sciences*, *40*(1), 413-439.
Guilmette, C., M. A. Smit, D. J. J. van Hinsbergen, D. Gürer, F. Corfu, B. Charette, M. Maffione, O. Rabeau, and D. Savard (2018), Forced subduction initiation recorded in the sole and crust of the Semail Ophiolite of Oman, *Nature Geoscience*, *11*(9), 688-695.
Gurnis, M., C. Hall, and L. Lavier (2004), Evolving force balance during incipient subduction, *Geochemistry, Geophysics, Geosystems*, *5*(7).
Haase, K. M., S. Freund, J. Koepke, F. Hauff, and M. Erdmann (2015), Melts of sediments in the mantle wedge of the Oman ophiolite, *Geology*.
Haase, K. M., S. Freund, C. Beier, J. Koepke, M. Erdmann, and F. Hauff (2016), Constraints on the magmatic evolution of the oceanic crust from plagiogranite intrusions in the Oman ophiolite, *Contributions to Mineralogy and Petrology*, *171*(5), 1-16.
Hacker, B. R., and J. L. Mosenfelder (1996), Metamorphism and deformation along the emplacement thrust of the Samail ophiolite, Oman, *Earth and Planetary Science Letters*, *144*(3-4), 435-451.
Hacker, B. R., J. L. Mosenfelder, and E. Gnos (1996), Rapid emplacement of the Oman ophiolite: Thermal and geochronologic constraints, *Tectonics*, *15*(6), 1230-1247.

Hall, C. E., M. Gurnis, M. Sdrolias, L. L. Lavier, and R. D. Müller (2003), Catastrophic initiation of subduction following forced convergence across fracture zones, *Earth and Planetary Science Letters*, *212*(1–2), 15-30.
Hanghøj, K., P. B. Kelemen, D. Hassler, and M. Godard (2010), Composition and genesis of depleted mantle peridotites from the Wadi Tayin massif, Oman ophiolite; Major and trace element geochemistry, and Os isotope and PGE systematics, *Journal of Petrology*, *51*(1-2), 201-227.
Hara, K., and T. Kurihara (2017), Radiolarian age and lithostratigraphy of Late Cretaceous pelagic sediments overlying basaltic extrusive rocks, northern Oman Mountains, *Ofioliti*, *42*(1), 21-38.
Hayman, N. W., M. Rioux, R. Anma, K. Tani, D. J. Dunkley, J. Crowley, and M. Schmitz (2019), Accretion and oxidation of a superfast-spread axial melt lens: TIMS and SIMS zircon analyses of the IODP Hole 1256D gabbros, *Lithos*, *348-349*, 105184.
Hiess, J., D. J. Condon, N. McLean, and S. R. Noble (2012), $^{238}U/^{235}U$ systematics in terrestrial uranium-bearing minerals, *Science*, *335*(6076), 1610-1614.
Huang, W.-L., and P. J. Wyllie (1975), Melting Reactions in the System NaAlSi3O8-KAlSi3O8-SiO2 to 35 Kilobars, Dry and with Excess Water, *The Journal of Geology*, *83*(6), 737-748.
Huang, W. L., and P. J. Wyllie (1981), Phase relationships of S-type granite with H2O to 35 kbar: Muscovite granite from Harney Peak, South Dakota, *Journal of Geophysical Research: Solid Earth*, *86*(B11), 10515-10529.
Ishikawa, T., K. Nagaishi, and S. Umino (2002), Boninitic volcanism in the Oman ophiolite: Implications for thermal condition during transition from spreading ridge to arc, *Geology*, *30*(10), 899-902.
Ishizuka, O., K. Tani, and M. K. Reagan (2014), Izu-Bonin-Mariana Forearc Crust as a Modern Ophiolite Analogue, *Elements*, *10*(2), 115-120.
Ishizuka, O., K. Tani, M. K. Reagan, K. Kanayama, S. Umino, Y. Harigane, I. Sakamoto, Y. Miyajima, M. Yuasa, and D. J. Dunkley (2011), The timescales of subduction initiation and subsequent evolution of an oceanic island arc, *Earth and Planetary Science Letters*, *306*(3), 229-240.
Jaffey, A. H., K. F. Flynn, L. E. Glendenin, W. C. Bentley, and A. M. Essling (1971), Precision measurement of half-lives and specific activities of ^{235}U and ^{238}U, *Physical Review C*, *4*(5), 1889-1906.
Juteau, T., M. Beurrier, R. Dahl, and P. Nehlig (1988), Segmentation at a fossil spreading axis: The plutonic sequence of the Wadi Haymiliyah area (Haylayn Block, Sumail Nappe, Oman), *Tectonophysics*, *151*(1–4), 167-197.
Karsten, J. L., E. M. Klein, and S. B. Sherman (1996), Subduction zone geochemical characteristics in ocean ridge basalts from the southern Chile Ridge: Implications of modern ridge subduction systems for the Archean, *Lithos*, *37*(2–3), 143-161.
Kelemen, P. B. (1986), Assimilation of Ultramafic Rock in Subduction-Related Magmatic Arcs, *The Journal of Geology*, *94*(6), 829-843.
Kelemen, P. B. (1990), Reaction Between Ultramafic Rock and Fractionating Basaltic Magma I. Phase Relations, the Origin of Calc-alkaline Magma Series, and the Formation of Discordant Dunite, *Journal of Petrology*, *31*(1), 51-98.
Kelemen, P. B., and M. S. Ghiorso (1986), Assimilation of peridotite in zoned calc-alkaline plutonic complexes: evidence from the Big Jim complex, Washington Cascades, *Contributions to Mineralogy and Petrology*, *94*(1), 12-28.

Kelemen, P. B., K. Koga, and N. Shimizu (1997), Geochemistry of gabbro sills in the crust-mantle transition zone of the Oman ophiolite: Implications for the origin of the oceanic lower crust, *Earth and Planetary Science Letters*, *146*(3-4), 475-488.
Kelemen, P. B., S. R. Hart, and S. Bernstein (1998), Silica enrichment in the continental upper mantle via melt/rock reaction, *Earth and Planetary Science Letters*, *164*(1), 387-406.
Kelemen, P. B., K. Hanghøj, and A. R. Greene (2003), One View of the Geochemistry of Subduction-Related Magmatic Arcs, with an Emphasis on Primitive Andesite and Lower Crust, in *Treatise on Geochemistry (First Edition)*, edited by H. D. Holland and K. K. Turekian, pp. 749-806, Elsevier, Oxford.
Kessel, R., M. W. Schmidt, P. Ulmer, and T. Pettke (2005), Trace element signature of subduction-zone fluids, melts and supercritical liquids at 120–180 km depth, *Nature*, *437*(7059), 724-727.
Kinzler, R. J. (1997), Melting of mantle peridotite at pressures approaching the spinel to garnet transition: Application to mid-ocean ridge basalt petrogenesis, *Journal of Geophysical Research: Solid Earth*, *102*(B1), 853-874.
Kinzler, R. J., and T. L. Grove (1992), Primary magmas of mid-ocean ridge basalts 2. Applications, *Journal of Geophysical Research: Solid Earth*, *97*(B5), 6907-6926.
Klein, E. M., and J. L. Karsten (1995), Ocean-ridge basalts with convergent-margin geochemical affinities from the Chile Ridge, *Nature*, *374*(6517), 52-57.
Kusano, Y., Y. Adachi, S. Miyashita, and S. Umino (2012), Lava accretion system around mid-ocean ridges: Volcanic stratigraphy in the Wadi Fizh area, northern Oman ophiolite, *Geochem. Geophys. Geosyst.*, *13*, Q05012.
Kusano, Y., M. Hayashi, Y. Adachi, S. Umino, and S. Miyashita (2014), Evolution of volcanism and magmatism during initial arc stage: constraints on the tectonic setting of the Oman Ophiolite, *Geological Society, London, Special Publications*, *392*(1), 177.
Kusano, Y., S. Umino, R. Shinjo, A. Ikei, Y. Adachi, S. Miyashita, and S. Arai (2017), Contribution of slab-derived fluid and sedimentary melt in the incipient arc magmas with development of the paleo-arc in the Oman Ophiolite, *Chemical Geology*, *449*, 206-225.
Kutterolf, S., J. C. Schindlbeck, A. H. F. Robertson, A. Avery, A. T. Baxter, K. Petronotis, and K.-L. Wang (2018), Tephrostratigraphy and Provenance From IODP Expedition 352, Izu-Bonin Arc: Tracing Tephra Sources and Volumes From the Oligocene to Recent, *Geochemistry, Geophysics, Geosystems*, *19*(1), 150-174.
Leng, W., and M. Gurnis (2011), Dynamics of subduction initiation with different evolutionary pathways, *Geochemistry, Geophysics, Geosystems*, *12*(12).
Leng, W., M. Gurnis, and P. Asimow (2012), From basalts to boninites: The geodynamics of volcanic expression during induced subduction initiation, *Lithosphere*, *4*(6), 511-523.
Lippard, S. J., A. W. Shelton, and I. G. Gass (1986), *The Ophiolite of Northern Oman*, 178 pp., Geological Society, London, London.
MacLeod, C. J., and D. A. Rothery (1992), Ridge axial segmentation in the Oman ophiolite: Evidence from along-strike variations in the sheeted dyke complex, *Geological Society, London, Special Publications*, *60*(1), 39-63.
MacLeod, C. J., C. J. Lissenberg, and L. E. Bibby (2013), "Moist MORB" axial magmatism in the Oman ophiolite: The evidence against a mid-ocean ridge origin, *Geology*.
Mattinson, J. M. (2005), Zircon U/Pb chemical abrasion (CA-TIMS) method: Combined annealing and multi-step partial dissolution analysis for improved precision and accuracy of zircon ages, *Chemical Geology*, *220*(1-2), 47-66.

Maunder, B., J. Prytulak, S. Goes, and M. Reagan (2020), Rapid subduction initiation and magmatism in the Western Pacific driven by internal vertical forces, *Nature Communications*, *11*(1), 1874.
McCulloch, M. T., R. T. Gregory, G. J. Wasserburg, and H. P. Taylor (1981), Sm-Nd, Rb-Sr, and $^{18}O/^{16}O$ isotopic systematics in an oceanic crustal section: Evidence from the Samail Ophiolite, *J. Geophys. Res.*, *86*(B4), 2721-2735.
McLean, N. M., J. F. Bowring, and S. A. Bowring (2011), An algorithm for U-Pb isotope dilution data reduction and uncertainty propagation, *Geochemistry, Geophysics, Geosystems*, doi: 10.1029/2010GC003478.
Moyen, J.-F., and G. Stevens (2006), Experimental Constraints on TTG Petrogenesis: Implications for Archean Geodynamics, in *Archean Geodynamics and Environments*, edited, pp. 149-175, American Geophysical Union.
Myers, J. D., B. D. Marsh, and A. K. Sinha (1985), Strontium isotopic and selected trace element variations between two Aleutian volcanic centers (Adak and Atka): implications for the development of arc volcanic plumbing systems, *Contributions to Mineralogy and Petrology*, *91*(3), 221-234.
Nicolas, A., and F. Boudier (2017), Emplacement of Semail–Emirates ophiolite at ridge–trench collision, *Terra Nova*, *29*(2), 127-134.
Nicolas, A., I. Reuber, and K. Benn (1988), A new magma chamber model based on structural studies in the Oman ophiolite, *Tectonophysics*, *151*(1-4), 87-105.
Nicolas, A., F. Boudier, and B. Ildefonse (1996), Variable crustal thickness in the Oman ophiolite: Implication for oceanic crust, *J. Geophys. Res.*, *101*(B8), 17941-17950.
Nicolas, A., F. Boudier, B. Ildefonse, and E. Ball (2000), Accretion of Oman and United Arab Emirates ophiolite – Discussion of a new structural map, *Marine Geophysical Research*, *21*(3), 147-180.
Nikolaeva, K., T. V. Gerya, and J. A. D. Connolly (2008), Numerical modelling of crustal growth in intraoceanic volcanic arcs, *Physics of the Earth and Planetary Interiors*, *171*(1), 336-356.
Pallister, J. S., and R. J. Knight (1981), Rare-earth element geochemistry of the Samail ophiolite near Ibra, Oman, *J. Geophys. Res.*, *86*(B4), 2673-2697.
Peacock, S. M. (1991), Numerical simulation of subduction zone pressure-temperature-time paths: constraints on fluid production and arc magmatism, *Philosophical Transactions of the Royal Society of London. Series A: Physical and Engineering Sciences*, *335*(1638), 341-353.
Peacock, S. M. (1996), Thermal and petrologic structure of subduction zones, *Subduction: top to bottom*, *96*, 119-133.
Pearce, J. A. (1989), High T/P metamorphism and granite genesis beneath ophiolite thrust sheets, *Ofioliti*, *14*(3), 195-211.
Pearce, J. A., T. Alabaster, A. W. Shelton, and M. P. Searle (1981), The Oman ophiolite as a Cretaceous arc-basin complex: Evidence and implications, *Philosophical Transactions of the Royal Society of London. Series A, Mathematical and Physical Sciences*, *300*(1454), 299-317.
Pearce, J. A., S. R. Van der Laan, R. J. Arculus, B. J. Murton, T. Ishi, D. W. Peate, and I. Parkinson (1992), Boninite and harzburgite from Leg 125 (Bonin-Mariana forearc): A case study of magma genesis during the initial stage of subduction, in *Proceedings of the Ocean Drilling Program, Scientific results*, edited by P. Fryer, J. A. Pearce and L. B. Stokking, pp. 623–659, Ocean Drilling Program, College Station, Texas.

Phipps Morgan, J., and Y. J. Chen (1993), The genesis of oceanic crust: Magma injection, hydrothermal circulation, and crustal flow, *Journal of Geophysical Research: Solid Earth*, *98*(B4), 6283-6297.
Prigent, C., S. Guillot, P. Agard, and B. Ildefonse (2018a), Fluid-Assisted Deformation and Strain Localization in the Cooling Mantle Wedge of a Young Subduction Zone (Semail Ophiolite), *Journal of Geophysical Research: Solid Earth*, *123*(9), 7529-7549.
Prigent, C., P. Agard, S. Guillot, M. Godard, and B. Dubacq (2018b), Mantle Wedge (De)formation During Subduction Infancy: Evidence from the Base of the Semail Ophiolitic Mantle, *Journal of Petrology*, *59*(11), 2061-2092.
Prigent, C., S. Guillot, P. Agard, D. Lemarchand, M. Soret, and M. Ulrich (2018c), Transfer of subduction fluids into the deforming mantle wedge during nascent subduction: Evidence from trace elements and boron isotopes (Semail ophiolite, Oman), *Earth and Planetary Science Letters*, *484*, 213-228.
Quick, J. E., and R. P. Denlinger (1993), Ductile deformation and the origin of layered gabbro in ophiolites, *Journal of Geophysical Research*, *98*(B8), 14015-14027.
Rapp, R. P., M. D. Norman, D. Laporte, G. M. Yaxley, H. Martin, and S. F. Foley (2010), Continent Formation in the Archean and Chemical Evolution of the Cratonic Lithosphere: Melt–Rock Reaction Experiments at 3–4 GPa and Petrogenesis of Archean Mg-Diorites (Sanukitoids), *Journal of Petrology*, *51*(6), 1237-1266.
Reagan, M. K., D. E. Heaton, M. D. Schmitz, J. A. Pearce, J. W. Shervais, and A. A. P. Koppers (2019), Forearc ages reveal extensive short-lived and rapid seafloor spreading following subduction initiation, *Earth and Planetary Science Letters*, *506*, 520-529.
Reagan, M. K., et al. (2010), Fore-arc basalts and subduction initiation in the Izu-Bonin-Mariana system, *Geochem. Geophys. Geosyst.*, *11*(3), Q03X12.
Reagan, M. K., et al. (2017), Subduction initiation and ophiolite crust: new insights from IODP drilling, *International Geology Review*, *59*(11), 1439-1450.
Reuber, I., P. Nehlig, and T. Juteau (1991), Axial segmentation at a fossil oceanic spreading centre in the Haylayn block (Semail nappe, Oman): Off-axis mantle diapir and advancing ridge tip, *Journal of Geodynamics*, *13*(2-4), 253-278.
Rioux, M., S. Bowring, M. Cheadle, and B. John (2015), Evidence for initial excess ^{231}Pa in mid-ocean ridge zircons, *Chemical Geology*, *397*, 143-156.
Rioux, M., S. A. Bowring, P. B. Kelemen, S. Gordon, F. Dudás, and R. Miller (2012), Rapid crustal accretion and magma assimilation in the Oman-U.A.E. ophiolite: High precision U-Pb zircon geochronology of the gabbroic crust, *Journal of Geophysical Research*, *117*.
Rioux, M., S. Bowring, P. Kelemen, S. Gordon, R. Miller, and F. Dudás (2013), Tectonic development of the Samail ophiolite: High-precision U-Pb zircon geochronology and Sm-Nd isotopic constraints on crustal growth and emplacement, *Journal of Geophysical Research*, *118*(5), 2085-2101.
Rioux, M., J. Garber, A. Bauer, S. Bowring, M. Searle, P. Kelemen, and B. Hacker (2016), Synchronous formation of the metamorphic sole and igneous crust of the Semail ophiolite: New constraints on the tectonic evolution during ophiolite formation from high-precision U-Pb zircon geochronology, *Earth and Planetary Science Letters*, *451*, p. 708–195.
Rioux, M., M. Benoit, I. Amri, G. Ceuleneer, J. Garber, M. Searle, and K. Leal (in review), The origin of felsic intrusions within the mantle section of the Samail ophiolite: Geochemical evidence for three distinct differentiation trends, *Journal of Geophysical Research*.

Robertson, A. H. F., S. Kutterolf, A. Avery, A. T. Baxter, K. Petronotis, G. D. Acton, C. Carvallo, and J. C. Schindlbeck (2018), Depositional setting, provenance, and tectonic-volcanic setting of Eocene–Recent deep-sea sediments of the oceanic Izu–Bonin forearc, northwest Pacific (IODP Expedition 352), *International Geology Review*, *60*(15), 1816-1854.
Rollinson, H. (2009), New models for the genesis of plagiogranites in the Oman ophiolite, *Lithos*, *112*(3-4), 603-614.
Rollinson, H. (2014), Plagiogranites from the mantle section of the Oman Ophiolite: models for early crustal evolution, *Geological Society, London, Special Publications*, *392*(1), 247-261.
Rollinson, H. (2015), Slab and sediment melting during subduction initiation: granitoid dykes from the mantle section of the Oman ophiolite, *Contributions to Mineralogy and Petrology*, *170*(3), 1-20.
Rollinson, H., and J. Adetunji (2013), Mantle podiform chromitites do not form beneath mid-ocean ridges: A case study from the Moho transition zone of the Oman ophiolite, *Lithos*, *177*, 314-327.
Schmidt, M. W., D. Vielzeuf, and E. Auzanneau (2004), Melting and dissolution of subducting crust at high pressures: the key role of white mica, *Earth and Planetary Science Letters*, *228*(1), 65-84.
Searle, M., and J. Cox (1999), Tectonic setting, origin, and obduction of the Oman ophiolite, *Geological Society of America Bulletin*, *111*(1), 104-122.
Searle, M., and J. Cox (2002), Subduction zone metamorphism during formation and emplacement of the Semail ophiolite in the Oman Mountains, *Geological Magazine*, *139*(3), 241-255.
Searle, M. P., and J. Malpas (1980), The structure and metamorphism of rocks beneath the Semail Ophiolite of Oman and their significance in ophiolite obduction, *Transactions of the Royal Society of Edinburgh, Earth Sciences*, *71*, 247–262.
Searle, M. P., and J. Malpas (1982), Petrochemistry and origin of sub-ophiolitic metamorphic and related rocks in the Oman Mountains, *Journal of the Geological Society, London*, *139*(3), 235-248.
Searle, M. P., D. J. Waters, H. N. Martin, and D. C. Rex (1994), Structure and metamorphism of blueschist-eclogite facies rocks from the northeastern Oman Mountains, *Journal of the Geological Society, London*, *151*(3), 555-576.
Searle, M. P., C. J. Warren, D. J. Waters, and R. R. Parrish (2004), Structural evolution, metamorphism and restoration of the Arabian continental margin, Saih Hatat region, Oman Mountains, *Journal of Structural Geology*, *26*(3), 451-473.
Searle, M. P., D. J. Waters, J. M. Garber, M. Rioux, A. G. Cherry, and T. K. Ambrose (2015), Structure and metamorphism beneath the obducting Oman ophiolite: Evidence from the Bani Hamid granulites, northern Oman mountains, *Geosphere*.
Sen, C., and T. Dunn (1995), Experimental modal metasomatism of a spinel lherzolite and the production of amphibole-bearing peridotite, *Contributions to Mineralogy and Petrology*, *119*(4), 422-432.
Shimizu, Y., S. Arai, T. Morishita, H. Yurimoto, F. Gervilla, S. Ishihara, W. E. Stephens, S. L. Harley, M. Arima, and T. Nakajima (2004), Petrochemical characteristics of felsic veins in mantle xenoliths from Tallante (SE Spain): an insight into activity of silicic melt within the mantle wedge, in *The Fifth Hutton Symposium on the Origin of Granites and Related Rocks*, edited, p. 0, Geological Society of America.

Soret, M., P. Agard, B. Dubacq, A. Plunder, and P. Yamato (2017), Petrological evidence for stepwise accretion of metamorphic soles during subduction infancy (Semail ophiolite, Oman and UAE), *Journal of Metamorphic Geology*, *35*(9), 1051-1080.
Soret, M., G. Bonnet, K. Larson, P. Agard, J. Cottle, B. Dubacq, and M. Button (2020), Slow subduction initiation forces fast ophiolite formation, in *Proceedings of the International Conference on Ophiolites and the Oceanic Lithosphere: Results of the Oman Drilling Project and Related Research* edited, p. 234, Sultan Qaboos University, Muscat, Sultanate of Oman, .
Spencer, C. J., A. J. Cavosie, T. D. Raub, H. Rollinson, H. Jeon, M. P. Searle, J. A. Miller, B. J. McDonald, N. J. Evans, and F. the Edinburgh Ion Microprobe (2017), Evidence for melting mud in Earth's mantle from extreme oxygen isotope signatures in zircon, *Geology*, *45*(11), 975-978.
Stern, R. J. (2004), Subduction initiation: spontaneous and induced, *Earth and Planetary Science Letters*, *226*(3–4), 275-292.
Stern, R. J., and S. H. Bloomer (1992), Subduction zone infancy: Examples from the Eocene Izu-Bonin-Mariana and Jurassic California arcs, *Geological Society of America Bulletin*, *104*(12), 1621-1636.
Stern, R. J., M. Reagan, O. Ishizuka, Y. Ohara, and S. Whattam (2012), To understand subduction initiation, study forearc crust: To understand forearc crust, study ophiolites, *Lithosphere*, *4*(6), 469-483.
Styles, M. T., R. J. Thomas, D. I. Schofield, K. M. Goodenough, E. R. Phillips, and A. R. Farrant (2006a), *Hatta, Sheet 50-5, 1:50,000*, Minestry of Energy, Petroleum and Minerals Sector, Minerals Department, United Arab Emirates.
Styles, M. T., et al. (2006b), *The geology and geophysics of the United Arab Emirates, Volume 2*, 351 pp., Ministry of Energy, United Arab Emirates, Abu Dhabi.
Syracuse, E. M., P. E. van Keken, and G. A. Abers (2010), The global range of subduction zone thermal models, *Physics of the Earth and Planetary Interiors*, *183*(1), 73-90.
Tilton, G. R., C. A. Hopson, and J. E. Wright (1981), Uranium-lead isotopic ages of the Samail ophiolite, Oman, with applications to Tethyan ocean ridge tectonics, *Journal of Geophysical Research*, *86*(B4), 2763–2775.
Tippit, P. R., E. A. Pessagno Jr., and J. D. Smewing (1981), The biostratigraphy of sediments in the volcanic unit of the Samail Ophiolite, *Journal of Geophysical Research: Solid Earth*, *86*(B4), 2756-2762.
Tsuchiya, N., T. Shibata, M. Yoshikawa, Y. Adachi, S. Miyashita, T. Adachi, N. Nakano, and Y. Osanai (2013), Petrology of Lasail plutonic complex, northern Oman ophiolite, Oman: An example of arc-like magmatism associated with ophiolite detachment, *Lithos*, *156–159*, 120-138.
Usui, Y., and S. Yamazaki (2010), Salvaging primary remanence from hydrothermally altered oceanic gabbros in the Oman ophiolite: A selective destructive demagnetization approach, *Physics of the Earth and Planetary Interiors*, *181*(1–2), 1-11.
van Hinsbergen, D. J. J., M. Maffione, L. M. T. Koornneef, and C. Guilmette (2019), Kinematic and paleomagnetic restoration of the Semail ophiolite (Oman) reveals subduction initiation along an ancient Neotethyan fracture zone, *Earth and Planetary Science Letters*, *518*, 183-196.
van Hinsbergen, D. J. J., et al. (2015), Dynamics of intraoceanic subduction initiation: 2. Suprasubduction zone ophiolite formation and metamorphic sole exhumation in context of absolute plate motions, *Geochemistry, Geophysics, Geosystems*, *16*(6), 1771-1785.
VanTongeren, J. A., P. B. Kelemen, and K. Hanghøj (2008), Cooling rates in the lower crust of the Oman ophiolite: Ca in olivine, revisited, *Earth and Planetary Science Letters*, *267*(1–2), 69-82.

Warren, C., R. Parrish, D. Waters, and M. Searle (2005), Dating the geologic history of Oman's Semail ophiolite: Insights from U-Pb geochronology, *Contributions to Mineralogy and Petrology*, *150*(4), 403-422.
Warren, C. J., R. R. Parrish, M. P. Searle, and D. J. Waters (2003), Dating the subduction of the Arabian continental margin beneath the Semail ophiolite, Oman, *Geology*, *31*(10), 889-892.
Watson, E. B., and T. M. Harrison (1983), Zircon saturation revisited: temperature and composition effects in a variety of crustal magma types, *Earth and Planetary Science Letters*, *64*(2), 295-304.
Whattam, S. A., and R. J. Stern (2011), The 'subduction initiation rule': a key for linking ophiolites, intra-oceanic forearcs, and subduction initiation, *Contributions to Mineralogy and Petrology*, *162*(5), 1031-1045.
Yamasaki, T., J. Maeda, and T. Mizuta (2006), Geochemical evidence in clinopyroxenes from gabbroic sequence for two distinct magmatisms in the Oman ophiolite, *Earth and Planetary Science Letters*, *251*(1–2), 52-65.
Yamato, P., P. Agard, B. Goffé, V. de Andrade, O. Vidal, and L. Jolivet (2007), New, high-precision P–T estimates for Oman blueschists: implications for obduction, nappe stacking and exhumation processes, *Journal of Metamorphic Geology*, *25*(6), 657-682.
Zhu, G., T. V. Gerya, D. A. Yuen, S. Honda, T. Yoshida, and J. A. D. Connolly (2009), Three-dimensional dynamics of hydrous thermal-chemical plumes in oceanic subduction zones, *Geochemistry, Geophysics, Geosystems*, *10*(11).

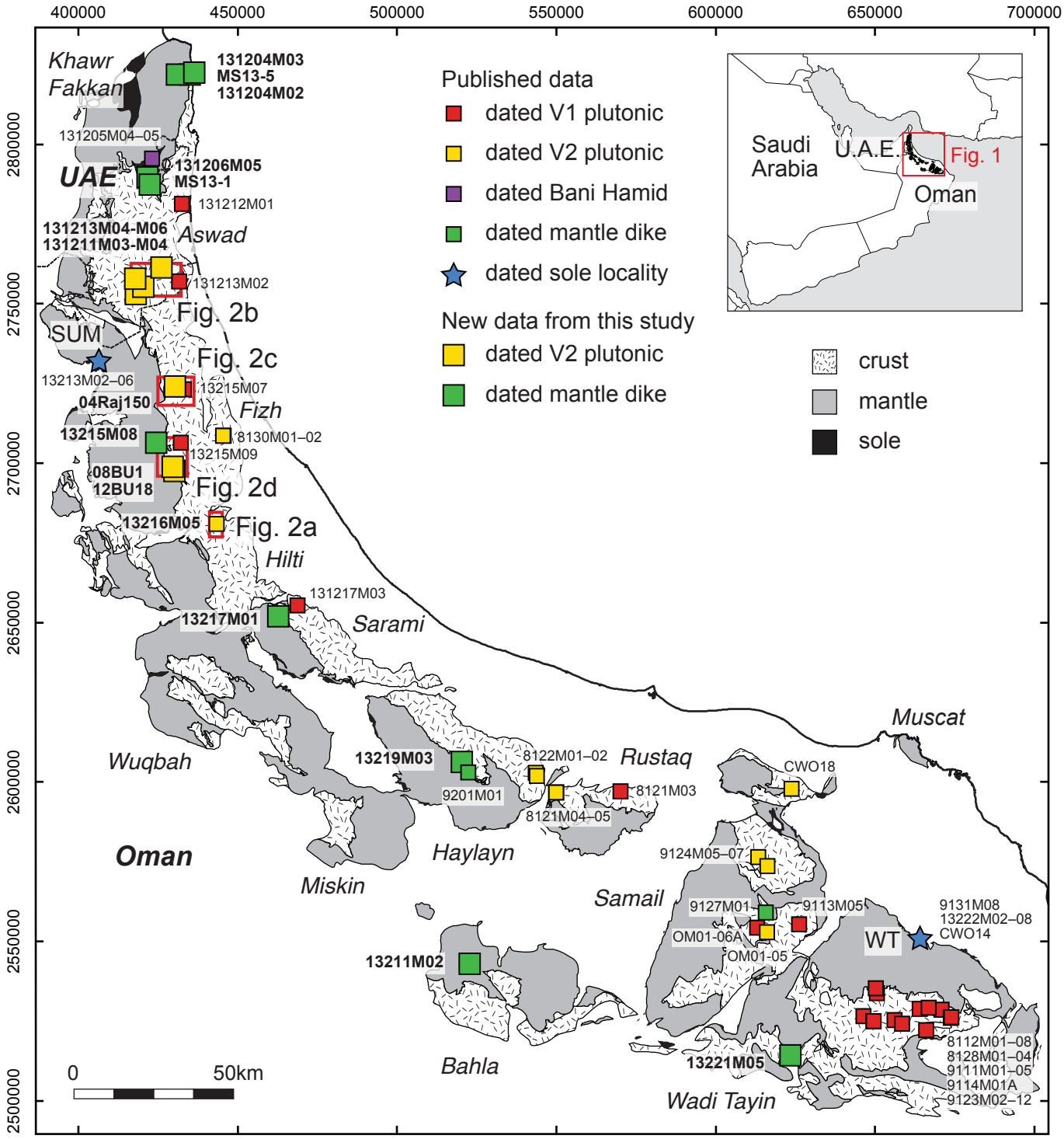
400000
450000
500000
550000
600000
650000
700000
2800000
2750000
2700000
2650000
2600000
2550000
2500000
Khawr Fakkan
131204M03
MS13-5
131204M02
131205M04–05
UAE
131206M05
MS13-1
131212M01
131213M04-M06
131211M03-M04
Aswad
131213M02
Fig. 2b
SUM
Fig. 2c
13213M02–06
13215M07
04Raj150
Fizh
13215M08
8130M01–02
13215M09
08BU1
12BU18
Fig. 2d
13216M05
Fig. 2a
Hilti
131217M03
13217M01
Sarami
Muscat
Wuqbah
13219M03
8122M01–02
Rustaq
CWO18
9201M01
8121M03
8121M04–05
Oman
9124M05–07
Haylayn
Miskin
Samail
9127M01
9113M05
9131M08
13222M02–08
CWO14
OM01-06A
OM01-05
WT
13211M02
8112M01–08
8128M01–04
9111M01–05
9114M01A
9123M02–12
Bahla
13221M05
Wadi Tayin
0
50km
Published data
dated V1 plutonic
dated V2 plutonic
dated Bani Hamid
dated mantle dike
dated sole locality
New data from this study
dated V2 plutonic
dated mantle dike
crust
mantle
sole
Saudi Arabia
U.A.E.
Oman
Fig. 1

Figure 1

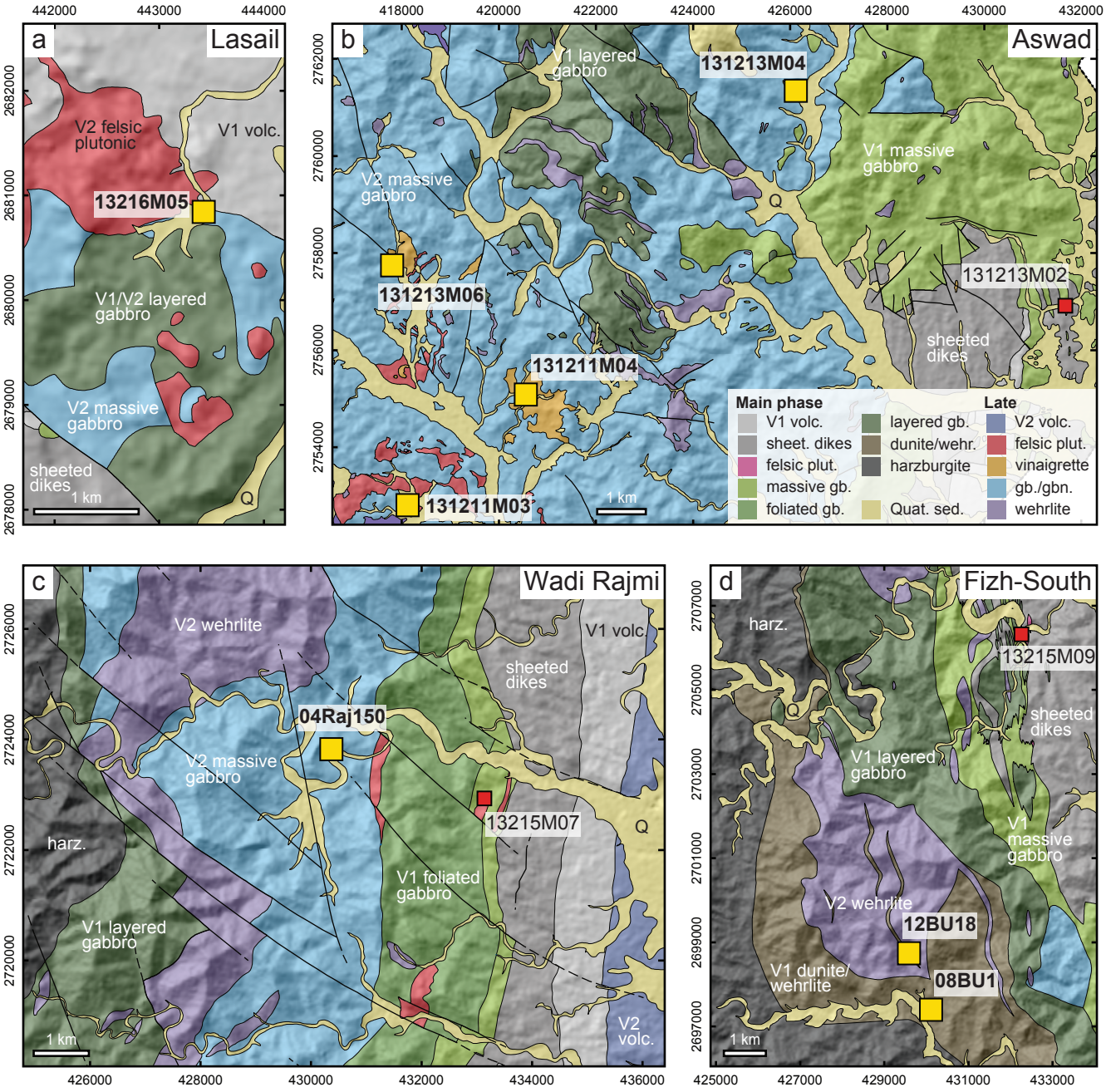
a
Lasail
V2 felsic plutonic
V1 volc.
13216M05
V1/V2 layered gabbro
V2 massive gabbro
sheeted dikes
Q
1 km
b
Aswad
V1 layered gabbro
131213M04
V1 massive gabbro
V2 massive gabbro
Q
131213M06
131213M02
sheeted dikes
131211M04
131211M03
1 km
Main phase
V1 volc.
sheet. dikes
felsic plut.
massive gb.
foliated gb.
layered gb.
dunite/wehr.
harzburgite
Quat. sed.
Late
V2 volc.
felsic plut.
vinaigrette
gb./gbn.
wehrlite
c
Wadi Rajmi
V2 wehrlite
V1 volc.
sheeted dikes
04Raj150
V2 massive gabbro
13215M07
Q
harz.
V1 foliated gabbro
V1 layered gabbro
V2 volc.
1 km
d
Fizh-South
harz.
13215M09
Q
sheeted dikes
V1 layered gabbro
V1 massive gabbro
V2 wehrlite
12BU18
V1 dunite/ wehrlite
08BU1
1 km

Figure 2

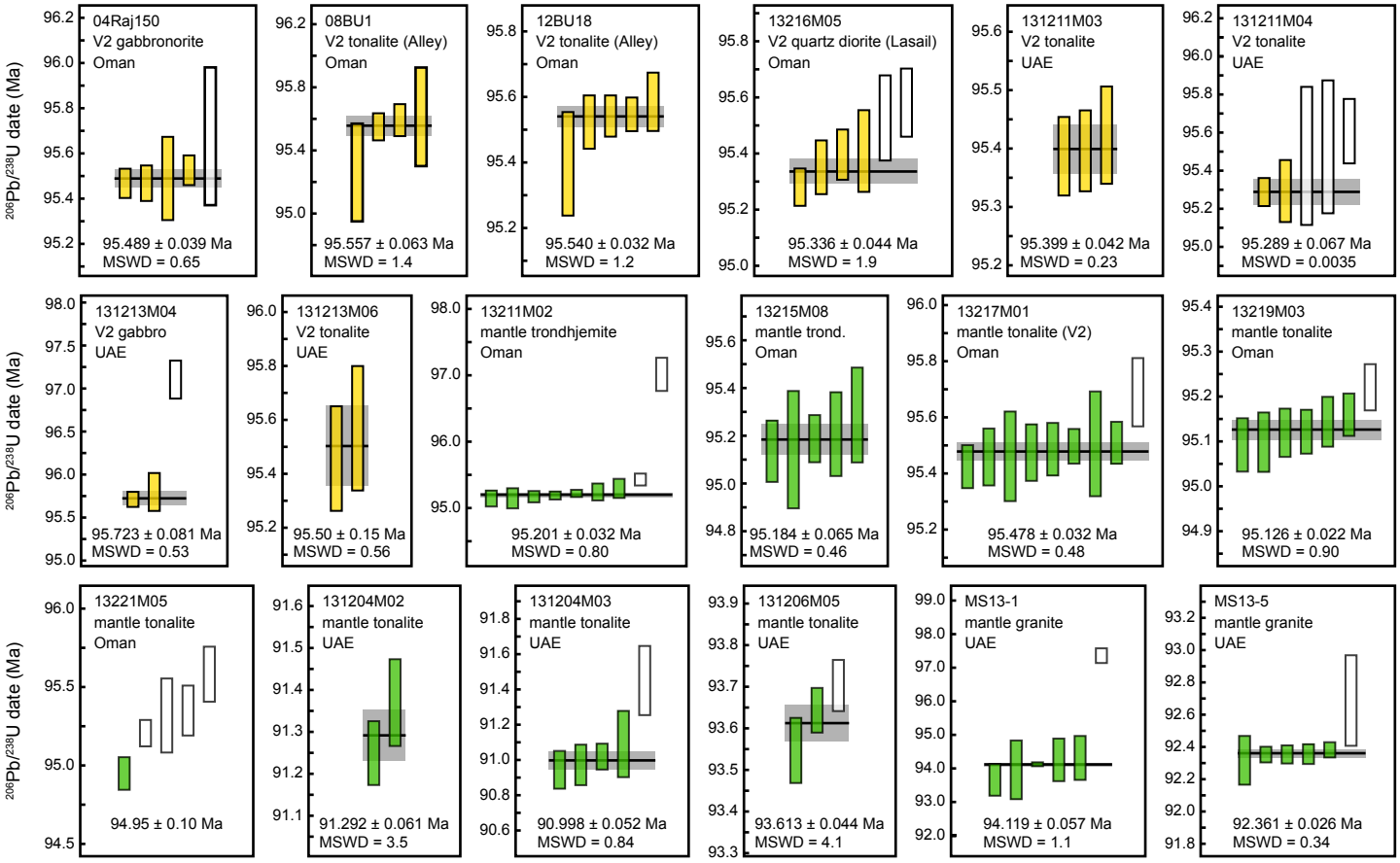
$^{206}Pb/^{238}U$ date (Ma)
04Raj150
V2 gabbronorite
Oman
95.489 ± 0.039 Ma
MSWD = 0.65
08BU1
V2 tonalite (Alley)
Oman
95.557 ± 0.063 Ma
MSWD = 1.4
12BU18
V2 tonalite (Alley)
Oman
95.540 ± 0.032 Ma
MSWD = 1.2
13216M05
V2 quartz diorite (Lasail)
Oman
95.336 ± 0.044 Ma
MSWD = 1.9
131211M03
V2 tonalite
UAE
95.399 ± 0.042 Ma
MSWD = 0.23
131211M04
V2 tonalite
UAE
95.289 ± 0.067 Ma
MSWD = 0.0035
131213M04
V2 gabbro
UAE
95.723 ± 0.081 Ma
MSWD = 0.53
131213M06
V2 tonalite
UAE
95.50 ± 0.15 Ma
MSWD = 0.56
13211M02
mantle trondhjemite
Oman
95.201 ± 0.032 Ma
MSWD = 0.80
13215M08
mantle trond.
Oman
95.184 ± 0.065 Ma
MSWD = 0.46
13217M01
mantle tonalite (V2)
Oman
95.478 ± 0.032 Ma
MSWD = 0.48
13219M03
mantle tonalite
Oman
95.126 ± 0.022 Ma
MSWD = 0.90
13221M05
mantle tonalite
Oman
94.95 ± 0.10 Ma
131204M02
mantle tonalite
UAE
91.292 ± 0.061 Ma
MSWD = 3.5
131204M03
mantle tonalite
UAE
90.998 ± 0.052 Ma
MSWD = 0.84
131206M05
mantle tonalite
UAE
93.613 ± 0.044 Ma
MSWD = 4.1
MS13-1
mantle granite
UAE
94.119 ± 0.057 Ma
MSWD = 1.1
MS13-5
mantle granite
UAE
92.361 ± 0.026 Ma
MSWD = 0.34

Figure 3

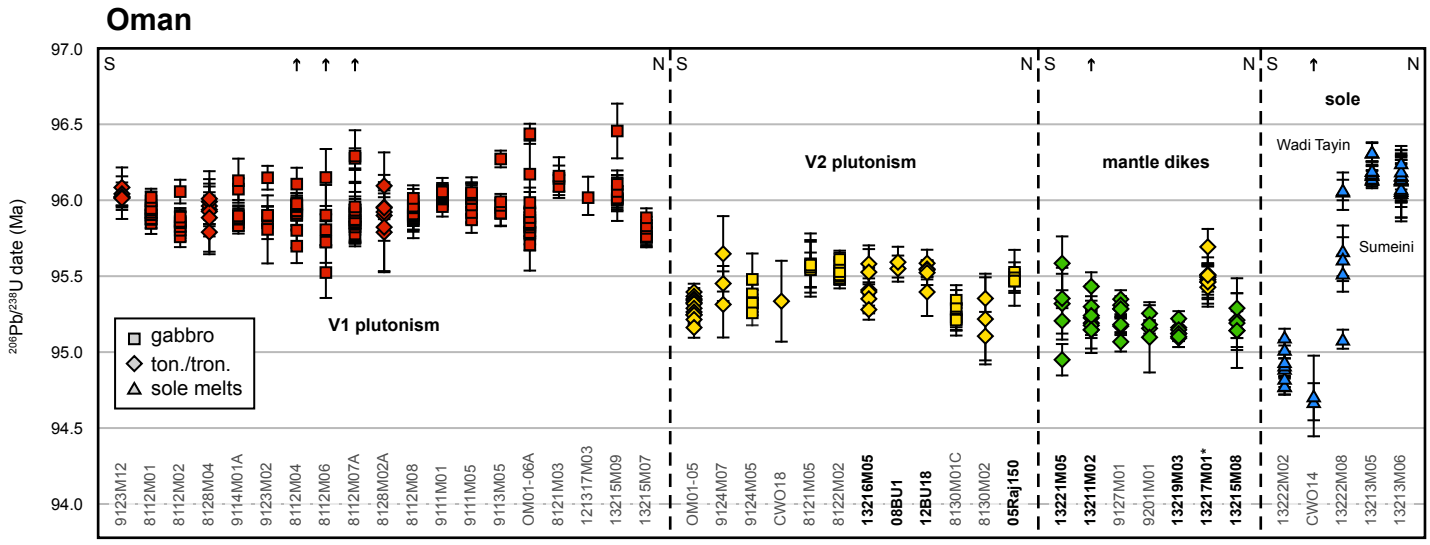
Oman
$^{206}Pb/^{238}U$ date (Ma)
97.0
96.5
96.0
95.5
95.0
94.5
94.0
S
N
V1 plutonism
V2 plutonism
mantle dikes
sole
Wadi Tayin
Sumeini
gabbro
ton./tron.
sole melts
9123M12
8112M01
8112M02
8128M04
9114M01A
9123M02
8112M04
8112M06
8112M07A
8128M02A
8112M08
9111M01
9111M05
9113M05
OM01-06A
8121M03
121317M03
13215M09
13215M07
OM01-05
9124M07
9124M05
CWO18
8121M05
8122M02
13216M05
08BU1
12BU18
8130M01C
8130M02
05Raj150
13221M05
13211M02
9127M01
9201M01
13219M03
13217M01*
13215M08
13222M02
CWO14
13222M08
13213M05
13213M06

Figure 4

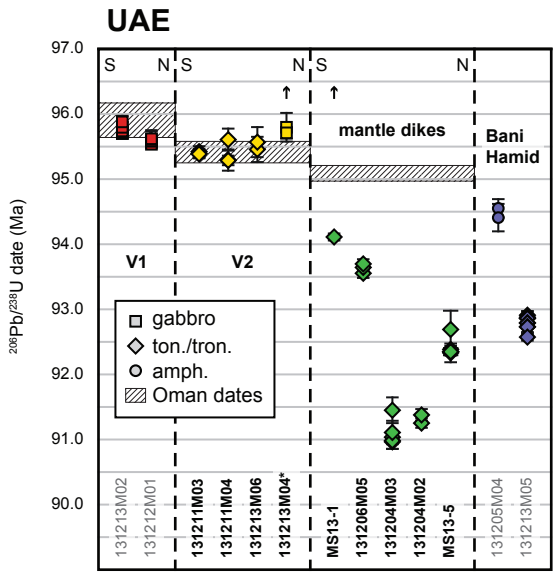
UAE
97.0
96.0
95.0
94.0
93.0
92.0
91.0
90.0
$^{206}Pb/^{238}U$ date (Ma)
S
N
S
N
S
N
mantle dikes
Bani Hamid
V1
V2
gabbro
ton./tron.
amph.
Oman dates
131213M02
131212M01
131211M03
131211M04
131213M06
131213M04*
MS13-1
131206M05
131204M03
131204M02
MS13-5
131205M04
131213M05

Figure 5

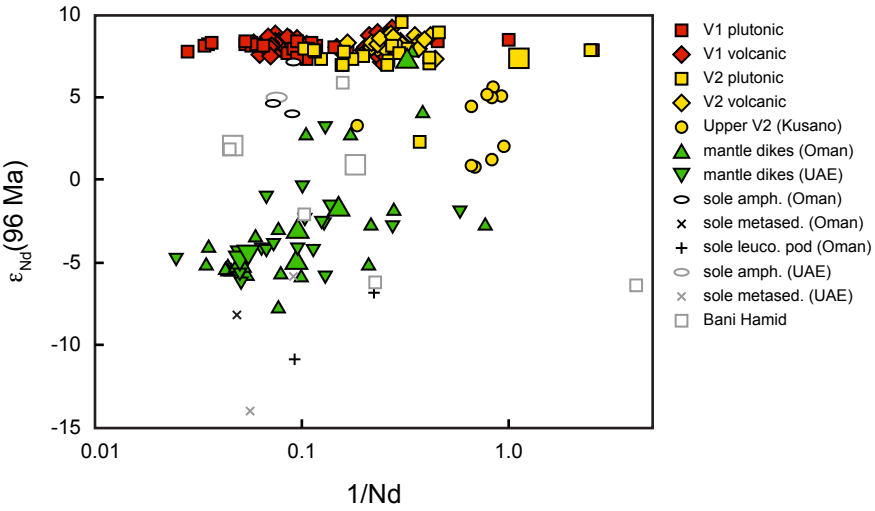
10
5
0
-5
-10
-15
0.01
0.1
1.0
1/Nd
εNd(96 Ma)
V1 plutonic
V1 volcanic
V2 plutonic
V2 volcanic
Upper V2 (Kusano)
mantle dikes (Oman)
mantle dikes (UAE)
sole amph. (Oman)
sole metased. (Oman)
sole leuco. pod (Oman)
sole amph. (UAE)
sole metased. (UAE)
Bani Hamid

Figure 6

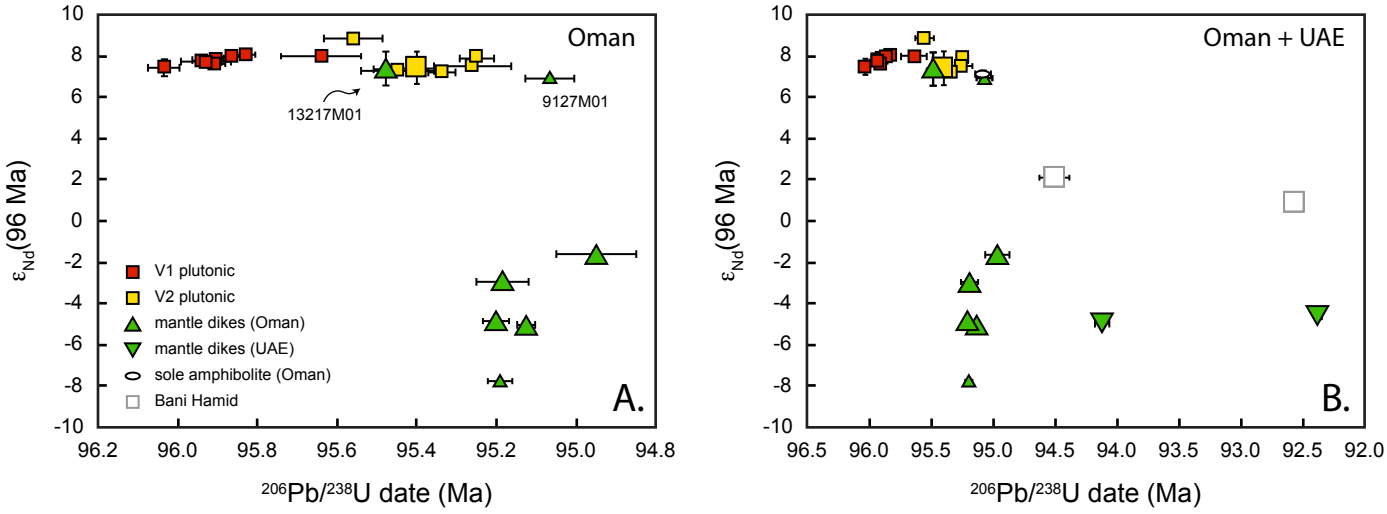
Oman
13217M01
9127M01
V1 plutonic
V2 plutonic
mantle dikes (Oman)
mantle dikes (UAE)
sole amphibolite (Oman)
Bani Hamid
A.
ε_{Nd}(96 Ma)
^{206}Pb/^{238}U date (Ma)
Oman + UAE
B.
ε_{Nd}(96 Ma)
^{206}Pb/^{238}U date (Ma)

Figure 7

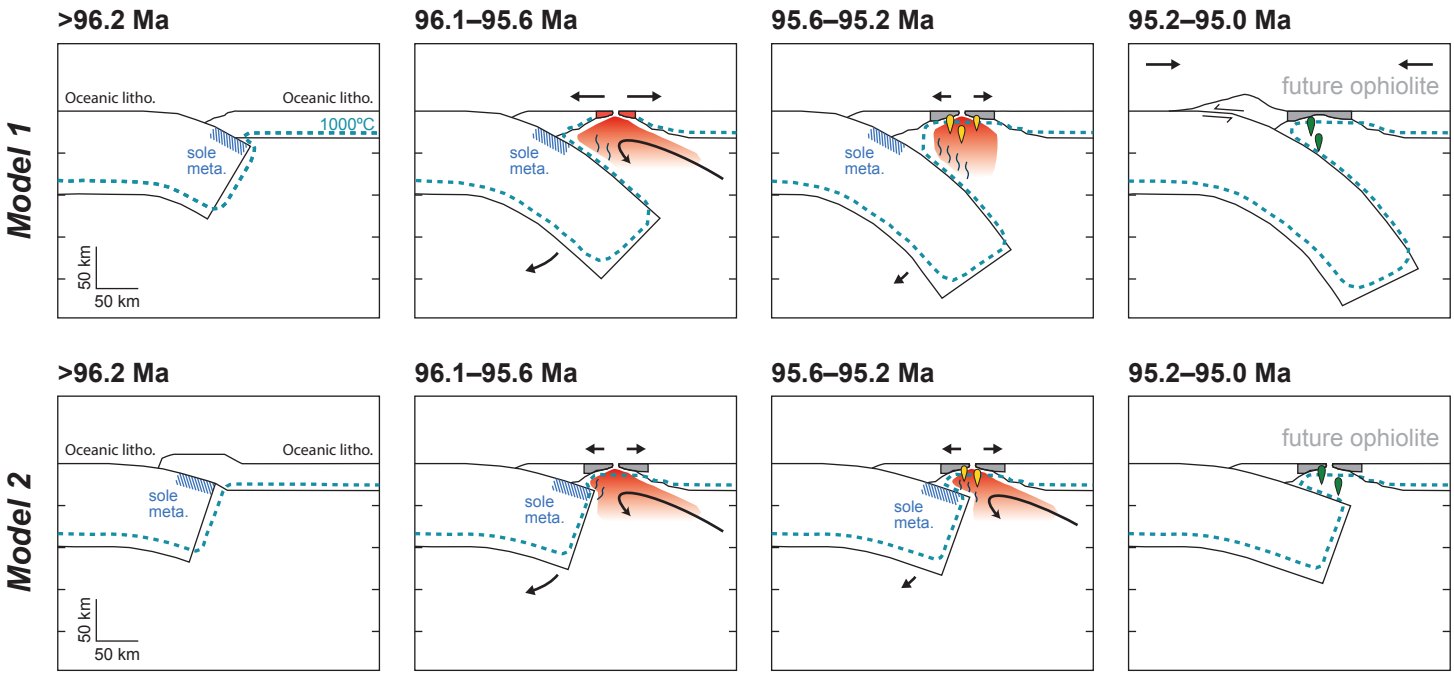

- Subduction initiation

- **V1 ridge magmatism**
- **Sole metamorphism**
- Slab rollback leads to decompression melting

- **V2 magmatism**
- Slab derived fluids/melts lead to flux melting of the wedge

- **Felsic mantle dikes**
- Slab melts intrude the ophiolite mantle

Figure 8

Journal of Geophysical Research

Supporting Information for

High-precision U-Pb zircon dating of late magmatism in the Samail ophiolite: A record of subduction initiation

Matthew Rioux[1,2,*], Joshua Garber[3], Michael Searle[4], Peter Kelemen[5], Sumio Miyashita[6], Yoshiko Adachi[7], Samuel Bowring[7]

[1] *Department of Earth Science, University of California, Santa Barbara, CA, 93106, USA*

[2] *Earth Research Institute, University of California, Santa Barbara, CA, 93106, USA*

[3] *Department of Geosciences, The Pennsylvania State University, University Park, PA 16803, USA*

[4] *Department of Earth Sciences, University of Oxford, Oxford, OX1 3AN, UK*

[5] *Department of Earth and Environmental Studies, Columbia University, Lamont Doherty Earth Observatory, Palisades, NY, 10964, USA*

[6] *Hokkaido Research Center of Geology, 58-7, Nopporo, Ebetsu, 069-0813, Japan*

[7] *Environmental Science Research Laboratory, Central Research Institute of Electric Power Industry, Abiko, Chiba, 270-1194, Japan*

[8] *Department of Earth, Atmospheric and Planetary Science, Massachusetts Institute of Technology, Cambridge, MA, 02139, USA*

[*] *corresponding author: rioux@eri.ucsb.edu*

Contents of this file

Additional Supporting Information (Files uploaded separately)

Introduction

The supplemental material includes text describing our interpretation of the U-Pb data for each sample and how samples were grouped into the V1 or V2 plutonic units (Text S1); Wetherill concordia plots for each of the dated samples (Figure S1); outcrop photos of dated samples with 'vinaigrette' textures (Figure S2); a table reporting single grain or grain fragment isotope dilution-thermal ionization mass spectrometry U-Pb zircon data (Table S1; xlsx) and a table reporting whole-rock Sm-Nd isotopic data (Table S2; xlsx). Analytical methods are described in the main text of this article.

Text S1.

Interpretation of the U-Pb dates

We report new U-Pb zircon dates from 18 samples. Detailed discussions of the results from each sample are provided below. In this discussion and the main text, we refer to calculated weighted mean dates for most samples. The weighted mean dates are a convenient way to estimate and discuss the crystallization age of the sample based on data from multiple fractions; however, the conclusions of this study do not change whether the crystallization age is estimated based on the weighted mean date or from the youngest fraction in each sample. In the following discussion, we note when the dataset from a sample includes one or more lower-precision analyses ($2\sigma \geq \pm 0.45$ Ma); in each sample, the lower-precision dates overlap within uncertainty with the more precise analyses (unless otherwise noted), but are excluded from the plots, discussions and calculated weighted mean dates in the main text, Supplementary Figure S1, and this discussion, for clarity. $^{206}Pb/^{238}U$ dates discussed here and throughout are corrected for initial exclusion of ^{230}Th, as described in the main text.

04Raj150, V2 oxide gabbronorite, Wadi Rajmi, Fizh massif: Five single-zircon fractions yielded $^{206}Pb/^{238}U$ dates of 95.68 ± 0.30 to 95.468 ± 0.065 Ma. All of the dates overlap within uncertainty and the four most precise dates ($2\sigma < \pm 0.3$ Ma) yield a weighted mean $^{206}Pb/^{238}U$ date of 95.489 ± 0.039 Ma (MSWD = 0.65).

08BU1, V2 tonalite, Fizh-S complex, Fizh massif: Four single-zircon fractions yielded $^{206}Pb/^{238}U$ dates of 95.61 ± 0.31 to 95.26 ± 0.31 Ma, with a weighted mean $^{206}Pb/^{238}U$ date of 95.557 ± 0.063 Ma (MSWD = 1.4).

12BU18, V2 tonalite, Fizh-S complex, Fizh massif: Five single-zircon fractions yielded $^{206}Pb/^{238}U$ dates of 95.585 ± 0.089 to 95.40 ± 0.16 Ma. All of the dates overlap within uncertainty and yield a weighted mean $^{206}Pb/^{238}U$ date of 95.540 ± 0.032 Ma (MSWD = 1.2).

13216M05, V2 quartz diorite, Lasail complex, Hilti massif: Six single-zircon fractions yielded $^{206}Pb/^{238}U$ dates of 95.58 ± 0.12 to 95.280 ± 0.067 Ma. There is a resolvable spread in dates. The four youngest analyses yield a weighted mean $^{206}Pb/^{238}U$ date of 95.336 ± 0.044 Ma (MSWD = 1.9), and we interpret this to be the best estimate of the crystallization age for this sample.

131211M03, V2 tonalite, Aswad massif: Three single-zircon fractions yielded $^{206}Pb/^{238}U$ dates of 95.423 ± 0.083 to 95.387 ± 0.067 Ma, and a weighted mean $^{206}Pb/^{238}U$ date of 95.399 ± 0.042 Ma (MSWD = 0.23).

131211M04, V2 tonalite, Aswad massif: Five single-zircon fractions yielded $^{206}Pb/^{238}U$ dates of 95.61 ± 0.17 to 95.288 ± 0.074 Ma. There is a resolvable spread in dates. The two youngest, precise dates ($2\sigma < \pm 0.3$ Ma) yield a weighted mean $^{206}Pb/^{238}U$ date of 95.289 ± 0.067 Ma (MSWD = 0.0035), and we interpret this to be the best estimate of the crystallization age for this sample. A single excluded lower precision analysis yielded a $^{206}Pb/^{238}U$ date of 94.3 ± 1.5 Ma.

131213M04, Fujairah gabbro (V2), Aswad massif: Three single-zircon fractions yielded $^{206}Pb/^{238}U$ dates of 97.10 ± 0.22 to 95.711 ± 0.088 Ma. The two younger dates overlap within uncertainty and yield a weighted mean $^{206}Pb/^{238}U$ date of 95.723 ± 0.081 Ma (MSWD = 0.53). We interpret the weighted mean date as the best estimate of the crystallization age of this sample, and the one older fraction as an inherited xenocrystic grain.

131213M06, V2 tonalite, Aswad massif: Two single-zircon fractions yielded $^{206}Pb/^{238}U$ dates of 95.57 ± 0.23 and 95.46 ± 0.19 Ma, with a weighted mean $^{206}Pb/^{238}U$ date of 95.50 ± 0.15 Ma. One excluded lower precision analysis yielded a $^{206}Pb/^{238}U$ date of 94.99 ± 0.54 Ma.

13211M02, trondhjemite dike intruding mantle harzburgite, Bahla massif: Nine single-zircon fractions yielded $^{206}Pb/^{238}U$ dates of 97.01 ± 0.25 to 95.14 ± 0.12 Ma. The seven youngest dates overlap within uncertainty and yield a weighted mean $^{206}Pb/^{238}U$ date of 95.201 ± 0.032 Ma (MSWD = 0.80). We interpret the weighted mean date as the best estimate of the crystallization age of this sample, and the two older fractions as inherited xenocrystic zircons.

13215M08, trondhjemite dike intruding mantle harzburgite, Fizh massif: Five single-zircon fractions yielded $^{206}Pb/^{238}U$ dates of 95.29 ± 0.20 to 95.14 ± 0.13 Ma, and a weighted mean $^{206}Pb/^{238}U$ date of 95.184 ± 0.065 Ma (MSWD = 0.46).

13217M01, tonalite dike intruding mantle harzburgite, Sarami massif: Nine single-zircon fractions yielded $^{206}Pb/^{238}U$ dates of 95.69 ± 0.12 to 95.424 ± 0.077 Ma. The eight youngest dates overlap within uncertainty and yield a weighted mean $^{206}Pb/^{238}U$ date of 95.478 ± 0.032 Ma (MSWD = 0.48). We interpret the weighted mean date as the best estimate of the crystallization age of this sample, and the single slightly older fraction as an inherited xenocrystic zircon.

13219M03, quartz diorite dike intruding mantle harzburgite, Haylayn massif: Seven single-zircon fractions yielded $^{206}Pb/^{238}U$ dates of 95.221 ± 0.051 to 95.092 ± 0.059 Ma. The six youngest dates overlap within uncertainty and yield a weighted mean $^{206}Pb/^{238}U$ date of 95.126 ± 0.022 Ma (MSWD = 0.90). We interpret the weighted mean date as the best estimate of the crystallization age of this sample, and the single slightly older fraction as an inherited xenocrystic zircon.

13221M05, tonalite dike intruding mantle harzburgite, Wadi Tayin massif: Five single-zircon fractions yielded $^{206}Pb/^{238}U$ dates of 95.58 ± 0.18 to 94.95 ± 0.10 Ma. The data define a spread of dates along concordia, and we interpret the youngest date (94.95 ± 0.10 Ma) as the best estimate of the crystallization age.

131204M02, tonalite dike intruding mantle harzburgite, Khor Fakkan massif: Two single-zircon fractions yielded $^{206}Pb/^{238}U$ dates of 91.37 ± 0.10 and 91.253 ± 0.076 Ma, with a weighted mean $^{206}Pb/^{238}U$ date of 91.292 ± 0.061 (MSWD = 3.5).

131204M03, tonalite dike intruding mantle harzburgite, Khor Fakkan massif: Five single-zircon fractions yielded $^{206}Pb/^{238}U$ dates of 91.45 ± 0.20 to 90.94 ± 0.11 Ma. The four youngest dates overlap within uncertainty and yield a weighted mean $^{206}Pb/^{238}U$ date of 90.998 ± 0.052 Ma (MSWD = 0.84). We interpret the weighted mean date as the best estimate of the crystallization age of this sample, and the single slightly older fraction as an inherited xenocrystic zircon.

131206M05, biotite tonalite dike intruding mantle harzburgite, Khor Fakkan massif: Three single-zircon fractions yielded $^{206}Pb/^{238}U$ dates of 93.703 ± 0.061 to 93.547 ± 0.0.078 Ma. The two youngest dates overlap within uncertainty and yield a weighted mean $^{206}Pb/^{238}U$ date of 93.613 ± 0.044 (MSWD = 4.1). Two excluded lower precision analyses yielded $^{206}Pb/^{238}U$ dates of 94.11 ± 0.45 Ma and 93.78 ± 0.51 Ma.

MS13-1, garnet, muscovite granite dike intruding mantle harzburgite, Khor Fakkan massif: The majority of the dated zircons had low radiogenic lead contents (≤ 1 pg) leading to imprecise results. Five of the datum define a cluster with a weighted mean $^{206}Pb/^{238}U$ date = 94.119 ± 0.057 (MSWD = 1.1). The weighted mean is dominated by a single precise analysis with a $^{206}Pb/^{238}U$ date of 94.124 ± 0.058 Ma. We interpret the weighted mean, which is almost identical to the date of the single precise analysis, to be the best estimate of the crystallization age of the sample. A second precise analysis yielded an older $^{206}Pb/^{238}U$ date of 97.36 ± 0.22 Ma, likely reflecting inheritance of xenocrystic older zircons.

MS13-5, garnet granite dike intruding mantle harzburgite, Khor Fakkan massif: Six single-zircon fractions yielded $^{206}Pb/^{238}U$ dates of 92.69 ± 0.28 to 92.32 ± 0.15 Ma. The five youngest dates overlap within uncertainty and yield a weighted mean $^{206}Pb/^{238}U$ date of 92.361 ± 0.026 Ma (MSWD = 0.34).

Grouping of the data

An important consideration in interpreting the U-Pb dates is determining what magmatic series the dated rocks are related to. In our previous work, we dated four samples from the northern Rustaq and southern Haylayn massifs—two gabbroic samples (gabbro and gabbronorite) and two adjacent felsic intrusions (tonalite and trondhjemite). The southern Haylayn massif contains abundant gabbronorite, which has been attributed to both closed system fractionation *[Juteau et al., 1988]* and hydration of the mantle wedge during initial subduction *[Yamasaki et al., 2006]*. Yamasaki et al. [2006] demonstrated that the later gabbronorite series is chemically similar to, and likely represents the intrusive equivalent of, the V2 Alley volcanic rocks in the area. We originally attributed the rocks we studied in the Rustaq and Haylayn massifs to propagation of a spreading ridge *[MacLeod and Rothery, 1992; Reuber et al., 1991]* during the V1 magmatic event *[Rioux et al., 2013; Rioux et al., 2016]*, and these samples recorded some of the youngest dates in the V1 series. Following the interpretations of Yamasaki et al. [2006], we have now shifted the data for the two gabbroic samples from this area (8121M05, 8122M02) from the V1 field to the V2 field in Figure 4; the felsic intrusions yielded lower-precision results and are excluded from the compilation.

Cited references are provided in the main text.

V2 plutonic—Oman

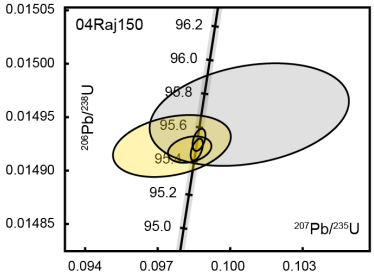

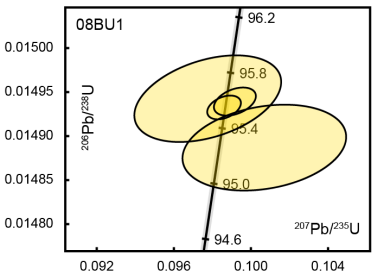

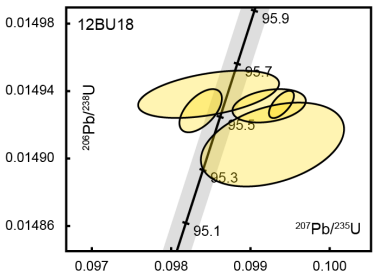

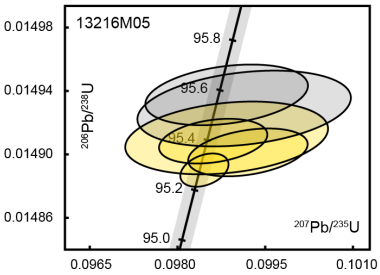

V2 plutonic—UAE

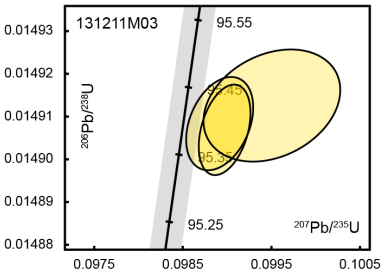

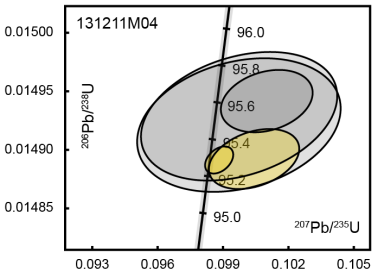

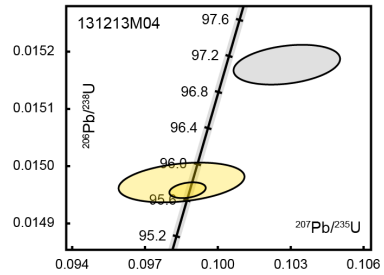

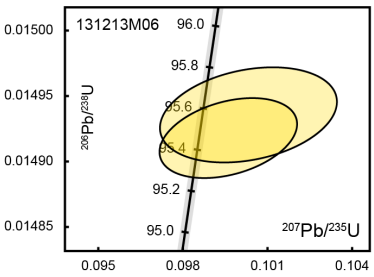

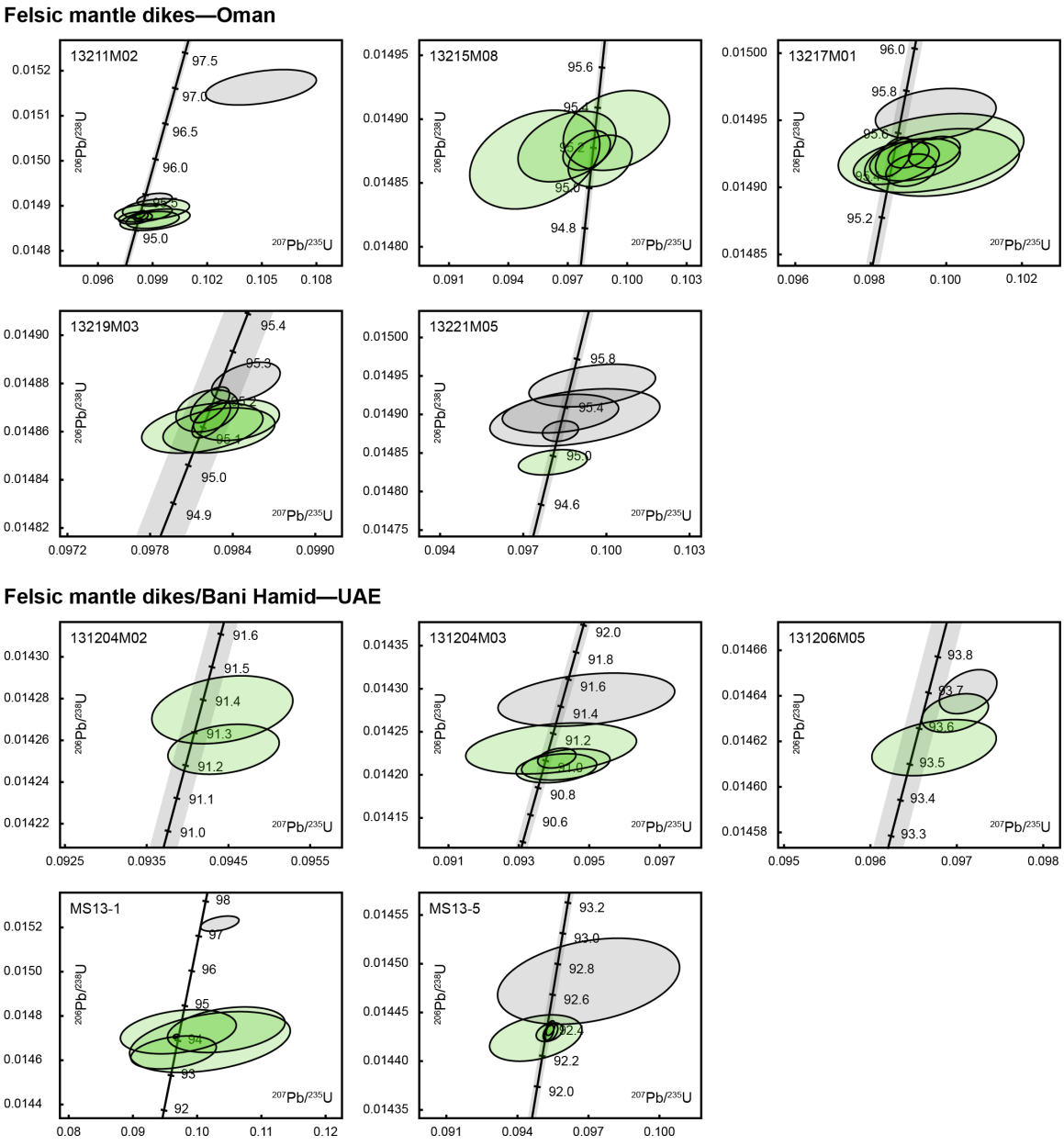

Figure S1. Wetherill concordia diagrams. Each datum is an analysis of a single zircon or zircon fragment. All data are corrected for initial ^{230}Th exclusion. Ages on concordia are in millions of years (Ma). Gray bands represent ± 2σ uncertainties on concordia based on decay constant uncertainties (Jaffey et al., 1971). Plots were generated using the ET_Redux software package (Bowring et al., 2011; McLean et al., 2011). Gray ellipses were excluded from the weighted mean calculations. For clarity, we excluded single zircon analyses with uncertainties ≥ ±0.45 Ma (Supplementary Text S1), with the exception of sample MS13-1—this sample yielded imprecise results and we plot all of the data.

Figure S2. Outcrop photos of 'vinaigrette' textures in samples 131211M04, and 131213M06.